ANL/RPG-94/1

Argonne National Laboratory
9700 South Cass Avenue
Argonne, Illinois 60439

RADIATION AND PHOTOCHEMISTRY SECTION
Annual Report
October 1992 - November 1993
Chemistry Division
Argonne National Laboratory

November 1993

Work performed under the auspices of the Office of Basic Energy Sciences
Division of Chemical Science, U.S. Department of Energy.

RADIATION AND PHOTOCHEMISTRY SECTION
Section Head: Alexander D. Trifunac

Radiation & Photochemistry Group

Group Leader:
Alexander D. Trifunac, Senior Chemist

Staff:
David M. Bartels, Chemist
Charles D. Jonah, Chemist
Yi Lin, Assistant Chemist
Myran C. Sauer, Jr., Chemist
David W. Werst, Assistant Chemist

Low-Energy Accelerator Facility (LEAF) Group

Group Leader:
Charles D. Jonah, Chemist

Staff:
George L. Cox, Engineering Specialist
Donald T. Ficht, Engineering Specialist
Allan C. Youngs, Engineering Assistant

Postdoctoral Fellows:
Keith Cromack
Elizabeth Piocos
Ilya Shkrob

Special Term Appointees:
Robert H. Lowers
Klaus H. Schmidt
Patricia D. Walsh

Visiting Scientists:
Ron Cooper, University of Melbourne, Melbourne, Australia
10/93
Ping Han, Biomedical Engineering Institute, Tianjin, China
3/93 - Present
Vadim V. Krongauz, DSM Desotech, Inc., Fiber Optic Materials, Elgi, IL
3/93
An-dong Liu, Radiation Research Centre, Beijing, China
3/90 - Present
Stephen Mezyk, Atomic Energy of Canada, Pinawa, Manitoba Canada
7/93

TABLE OF CONTENTS

Research Highlights

October 1992 - November 1993

The following survey of the research activities of the Radiation Chemistry and Photochemistry Section is representative of highlights of the past year rather than a comprehensive account. For more detailed accounts of the activities described herein, see the articles listed in *Publications* and *Submissions* at the end of the report, or contact the author(s) indicated.

I. REACTIVE INTERMEDIATES IN THE CONDENSED PHASE: RADIATION CHEMISTRY AND PHOTOCHEMISTRY

A. D. Trifunac, D. M. Bartels, M. V. Barnabas, K. R. Cromack, C. D. Jonah, Y. Lin, A.-D. Liu, P. Han, M. C. Sauer, Jr., I. A. Shkrob, K. H. Schmidt, D. W. Werst, P. D. Walsh

Outside Collaborators: *R. Cooper, S. Mezyk, P. W. Percival, E. Roduner, C. Romero*

The research described in this survey represents a multifaceted and comprehensive approach to the study of transient intermediates and chemistry induced by energetic radiation. The goal is to determine the fundamental chemistry that occurs when ionizing or photoionizing radiation interacts with condensed-phase matter. The various short-lived intermediates, radicals, radical ions, electrons, and excited states all play a role in transforming high energy from photons and particles into different stable chemical products.

The simultaneous goals of this research are (1) an understanding of the chemical transformations induced by energetic radiation via the delineation of the overall framework of reactions; (2) the identification and description of reactions of transient species; and (3) the development of novel tools to allow better pursuit of such elusive reaction intermediates. State-of-the-art electron accelerators, ultrafast laser techniques, and novel detection means for the study of ultrafast processes and transient species are continuously being developed and improved.

This work has revealed the ubiquitous role of radical ions in their earliest observable time frame. Ion-molecule reactions play a very prominent role. The energy content of the radical cation determines its reactivity; for example, only electronically excited aromatic radical cations undergo ion-molecule reactions. Diffusion and molecular transport in general, as well as charge transport, are being examined at very low temperatures for the first time.

The use of novel microreactor/matrix materials such as zeolites allows unprecedented control of ion chemistry. We can observe and control multitudes of radical cation transformations, many of which were previously observed in the gas phase. Many radical cation processes that are photodriven in other matrices occur in zeolites without photochemical excitation.

This survey is presented in two major parts. Part A describes several research efforts in which we study *ions, excited states, and other transients in the condensed phase.* These include studies of radical cations and ion-molecule reactions by the techniques of magnetic resonance, picosecond emission, and picosecond absorption, which probe the role of ions in high-energy chemistry, and studies of ions and their reactivity in specialized matrices such as freons and zeolites.

Part B outlines the work on the *role of solvents in chemical reactivity.* Hydrogen and deuterium atoms have been used as probes of the short-time events in the radiation chemistry of water. The nature of the solvation structure around hydrated electrons has been compared with that of classical monatomic ions by way of thermodynamic and transport properties. In a study in which ions are produced by both laser excitation and pulse radiolysis, we examine the dynamics of solvent reorganization around transient ions.

Some of the highlights of the past year are:

(1) Observations of ion-molecule reactions of excited aromatic cations via flash photolysis and transient dc conductivity.

(2) Study of anion solvation reveals the significant role of solvent molecular structure.

(3) Zeolite matrices have allowed observation of a remarkable range of C_7H_8 radical cation chemistry, including the first direct EPR observation of the elusive quadricyclane radical cation.

(4) The study of H-atom reaction with O_2, I^- and comparison of the diffusion of H, D, and muonium in ice, continue to expand the use of this remarkable probe.

A. Chemistry of Ions in the Condensed Phase

A. D. Trifunac, C. D. Jonah. D. W. Werst, M. C. Sauer, Jr., K. R. Cromack, M. V. Barnabas, Y. Lin, A. D. Liu, I. A. Shkrob, R. Cooper

1. Zeolite Control of Radical Cation Reactions

A. D. Trifunac, D. W. Werst, M. V. Barnabas, K. R. Cromack

Radical cations of simple organic molecules are very short-lived in the condensed phase and thus are studied by fast time-resolved methods or in solid matrices that are capable of providing a large degree of stabilization. The matrix used for radical cation studies must possess at a minimum two attributes: it must trap electrons indefinitely, and it must be relatively chemically inert. Ion-molecule reactions of radical cations are ubiquitous in the condensed phase. The control of ion-molecule reactions requires isolation of the radical cations from parent molecules or other reactive neutrals. Matrix molecules in which the radical cations and unoxidized substrate molecules are diluted must be unreactive. Examples of inert matrices that prevent rapid ion recombination include solid inert gases with added electron acceptors, such as halocarbons and SF_6.

Zeolites possess several additional attributes conducive to the control and study of radical cation reactivity. Zeolites are crystalline solids and as such do not restrict the range of temperature studies as has been experienced with other matrices because of low melting point. The size-selective ability of zeolites plays a central role in isolating radical cations and neutral substrate molecules. Their pore dimensions limit the amplitude of possible molecular motions such as conformational changes and molecular rearrangements. Depending on the size of the substrate molecules, the motional freedom within a zeolite cavity might be intermediate between that characteristic of a frozen matrix and that of the liquid phase, or it may lie near either extreme. The remarkable range of synthetic possibilities with aluminosilicates provides another variable, that is, tunability of matrix ion interactions. Not only can pore sizes and channel dimensions be changed, but, within an isomorphous family of zeolites, polarity or acidity can be varied as well. In this way, specific electronic interactions between the matrix and radical cations can be enhanced.

We have studied several hydrocarbon radical cations in pentasil-type zeolites by variable-temperature EPR. The radical cation of the adsorbed hydrocarbon is formed by radiolysis (γ rays or fast electrons) at a temperature between 4.2 and 77 K. By carefully controlled annealing of the sample and by observing the EPR spectrum as a function of temperature, we are able to follow the reaction dynamics of the radical cation and observe both unimolecular and ion-molecule reactions. The radical cations reported here all show reaction behavior in zeolites different from that in freon matrices.

a. Elimination Reactions of Branched Alkane Radical Cations

The radical cations of methyl-substituted butanes have been previously studied in freon matrices, and, except for the hexamethylethane radical cation, their thermal and photoinduced reactions have been enumerated. In the absence of light, ion-molecule reactions take place to produce alkyl radicals by deprotonation of the parent cations. Photoexcitation produces exclusively the olefin radical cation by elimination of CH_4. We studied the reactions of the radical cations of 2,2,3-trimethylbutane (TMB) and hexamethylethane (HME) in Na-ZSM-5 zeolite with a SiO_2/Al_2O_3 ratio of 40.

Irradiation of TMB (.5-5 wt.%) in ZSM-5 at 77 K gave rise to the six-line spectrum (a = 31 G). This signal persisted to some degree to at least 170 K. Decay of the $TMB^{\bullet+}$ spectrum when the sample was annealed to 150-200 K was accompanied by the appearance of a multiplet spectrum with a hyperfine coupling constant of 17.2 G. The new signal was assigned to the tetramethylethylene radical cation. Thus, $TMB^{\bullet+}$ undergoes thermal elimination of CH_4 in the zeolite. In contrast, methane elimination from $TMB^{\bullet+}$ in the freon matrix requires photoexcitation.

Coexisting with the $TME^{\bullet+}$ signal in the annealed TMB samples is the EPR spectrum of the neutral radical, $(CH_3)_3CC^{\bullet}(CH_3)_2$ (a = 22.5 G), that forms as the product of the ion-molecule reaction between $TMB^{\bullet+}$ and neutral parent molecules. This radical eventually becomes the dominant species in the spectrum above 200 K. Scheme I-1 shows the processes that $TMB^{\bullet+}$ undergoes in ZSM-5.

$HME^{\bullet+}$, which lacks a tertiary C-H bond to facilitate elimination of CH_4, undergoes bond scission at the

central C-C bond. This reaction has not been reported in freon matrices. The seven-line spectrum (a = 31 G) of $HME^{\bullet+}$ that is observed in the zeolite after irradiation at 77 K is replaced upon annealing, >125 K, by the spectrum of the 2-methylallyl radical. The 2-methylallyl radical is the expected deprotonation product of the isobutene radical cation fragment that results from dissociation of $HME^{\bullet+}$ at the central C-C bond. This reaction sequence is depicted in Scheme I-2.

The spin density in methylbutane radical cations is highest in the central C-C bond. For $HME^{\bullet+}$, this is also the most labile bond. We have shown that scission of the central C-C bond does not occur in methylbutane radical cations that possess one or more tertiary C-H bonds. The central C-C bond in $HME^{\bullet+}$ is probably weaker than in less substituted butane cations because of greater steric repulsion between methyl groups. The dissociation mode may also depend on the relative facility of a concerted elimination process, such as methane elimination.

b. Isomerization of a Diene Radical Cation

The radical cation of 1,4-cyclohexadiene is stable in the freon matrix at 77 K. Shida et al. showed that annealing in $CFCl_3$ led to the decay of the parent radical cation and to the formation of the cyclohexadienyl radical as a result of ion-molecule reactions between the 1,4-cyclohexadiene radical cations and neutral parent molecules. On the other hand, when the 1,4-cyclohexadiene radical cation in $CFCl_3$ was irradiated with light ($\lambda > 700$ nm) to excite the intramolecular charge-resonance transition, it was shown to undergo isomerization to the 1,3-cyclohexadiene radical cation.

Figure 1-1 shows the EPR spectrum observed at 100 K after 77 K irradiation of a 2% sample of 1,4-cyclohexadiene in Na-ZSM-5 (SiO_2/Al_2O_3 = 170). The same spectrum was obtained when the same zeolite was loaded with 1,3-cyclohexadiene and then irradiated (Figure 1). The spectra are well simulated with the same hyperfine coupling constants used for the 1,3-cyclohexadiene radical cation in the freon matrix. Thus, the isomerization reaction 1,4-cyclohexadiene$^{\bullet+}$ → 1,3-cyclohexadiene$^{\bullet+}$ proceeds without the aid of light in the zeolite.

When the samples containing the 1,3-cyclohexadiene radical cation are annealed above 110 K, an irreversible change occurs to produce the cyclohexadienyl radical. The neutral radical is the product of ion-molecule reactions between the 1,3-cyclohexadiene radical cation and unoxidized substrate molecules, eq. 1. This reaction proceeds whether the substrate molecules are 1,4-cyclohexadiene or 1,3-cyclohexadiene. The product radical is the same in either case.

$$1,3\text{-}C_6H_8^{\bullet+} + 1,4\text{-}C_6H_8 \text{ (or } 1,3\text{-}C_6H_8) \rightarrow C_6H_7^{\bullet} \quad (1)$$

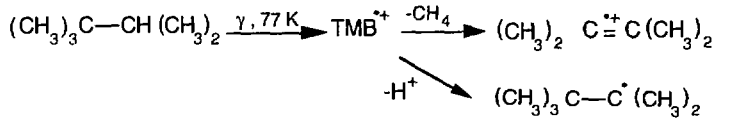

Scheme I-1

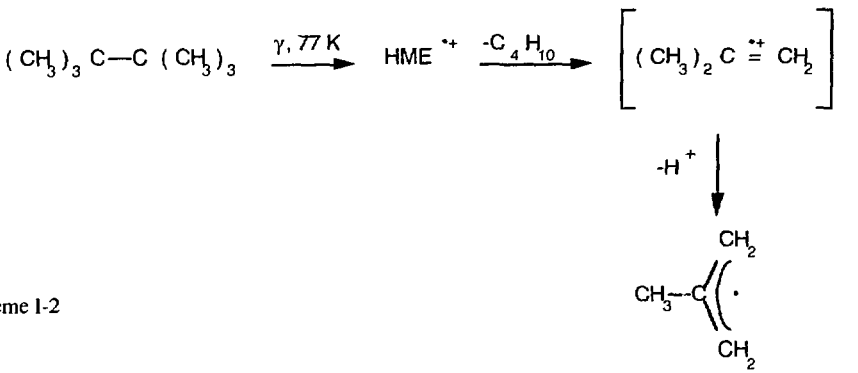

Scheme I-2

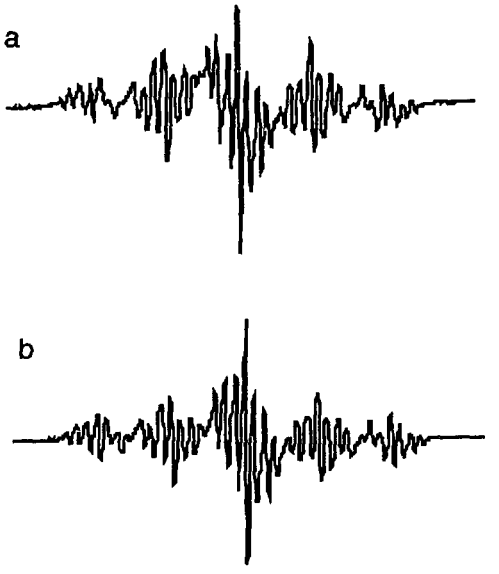

Figure 1. (a) EPR spectrum observed at 100 K after 77 K irradiation of 2%1,4-cyclohexadiene adsorbed on Na-ZSM-5. (b) EPR spectrum observed at 90 K after 77 K irradiation of 1.5% 1,3-cyclohexadiene adsorbed on Na-ZSM-5.

When different isomers produce distinguishable product radicals (e.g., as in the case of linear alkenes), the radical cation isomerization (thermal or photo-driven) followed by ion-molecule reaction can differentiate between two possible reaction mechanisms: proton transfer from the cation to the neutral and hydrogen-atom transfer from the neutral to the cation. Experiments are usually ambiguous on this point, and we expect to be able to make use of isomerization reactions to study the outcome of reactions of a given radical cation with different reaction partners. Ion-molecule reactions with the necessary asymmetry will reveal whether the radical product is derived from the radical cation (proton-transfer mechanism) or the neutral substrate molecule (hydrogen-atom transfer).

c. Transformations of $C_7H_8^{\bullet+}$ Family

It is hoped that zeolites with their unique properties will allow observations of many unstable radical cations that have eluded observation in other matrices. One such radical cation that we have studied in zeolites is the quadricyclane radical cation. Quadricyclane$^{\bullet+}$ is a member of the extensively studied $C_7H_8^{\bullet+}$ family of cations. Investigations of $C_7H_8^{\bullet+}$ species have been carried out in the gas phase and in the condensed phase and have revealed many excess-energy and photo-driven processes, including several isomerization reactions. Under most conditions, oxidation of quadricyclane yields the rearranged radical cation of norbornadiene, which is estimated to be more stable by approximately 10-12 kcal mol^{-1}. Previous efforts to observe quadricyclane$^{\bullet+}$ in freon matrices at 4.2 K were unsuccessful.

Utilizing our newly developed experimental capability for low-temperature in situ irradiation of samples in the EPR spectrometer, we have investigated the reactions of the quadricyclane radical cation, $1^{\bullet+}$, and the related norbornadiene radical cation, $2^{\bullet+}$, from 4.2 K and at higher temperatures. In zeolites, we have made several observations that are unique when compared to studies of C_7H_8 radical cations in other media: (1) A reverse Diels-Alder reaction gave rise to the cyclopentadiene radical cation in a thermal process, contrary to the expectation that this reaction is only photochemically allowed. (2) The bicyclo[3.2.0]hepta-2,6-diene radical cation is produced in small yield upon oxidation of quadricyclane or norbornadiene. (3) Some evidence has been gained for the stabilization of the quadricyclane radical cation in zeolites at very low temperatures.

Over most of the temperature range from 4.2 K to above 200 K, the dominant EPR signal after radiolysis of 1 or 2 in zeolites is that due to the norbornadiene radical cation (8.0 G(4H), 3.0 G(2H)). As the sample temperature is slowly increased, various reaction products are observed. One thermally activated reaction produces the cyclopentadiene radical cation, $4^{\bullet+}$, (24 G(4H), 14 G(2H)). The cyclopentadiene radical cation was observed after 200 K annealing of a sample in Na-ZSM-5 with a SiO_2/Al_2O_3 ratio of 170. However, it was not observed in ZSM-5 zeolites of lower polarity (i.e., higher SiO_2/Al_2O_3 ratio).

The cyclopentadiene radical cation was observed from the radiolysis of quadricyclane and norbornadiene. Its formation represents a (3+2) cycloreversion, which, as discussed by Bauld, is a thermally forbidden radical cation pericyclic reaction. This reaction has never been observed in the condensed phase before. It clearly proceeds thermally in the zeolite. If the exothermicity of the electron transfer from substrate molecules to the matrix holes activated the reaction,

then the formation of $4^{\bullet+}$ would be independent of temperature and would be observed immediately following irradiation. This was not the case.

The bicyclo[3.2.0]hepta-2,6-diene radical cation, $3^{\bullet+}$, (41.5 G(H), 31.6 G(H), 22.5 G(H), 4.5 G(H)) is produced upon irradiation, albeit in small yield (<5%), of quadricyclane or norbornadiene in polar Na-ZSM-5 zeolites, even at 4.2 K. In contrast, the 77 K radiolysis of quadricyclane and norbornadiene in freons gave the $3^{\bullet+}$ product only in the case of the former, especially under conditions of high dilution. Production of $3^{\bullet+}$ from norbornadiene was possible in the freon matrix only with photobleaching.

These results raise questions about the state of the radical cation precursor of the various radical cation products that are observed in zeolites and the influence of the zeolite matrix on reactions. The fact that processes are observed that in other media are photo-induced implies the involvement of excited states. In the case of the transformation to $3^{\bullet+}$, it is possible that the exothermicity of hole transfer from the matrix to substrate molecules provides the necessary excitation to drive the reaction. However, only a small percentage of parent cations react to give $3^{\bullet+}$. Thus, energy relaxation to yield the ground-state parent cation must compete favorably with rearrangement.

In the freon matrix this competition is very sensitive to the local environment. The strong concentration dependence of the yield of $3^{\bullet+}$ in freon matrices was explained by others by assuming that energy dissipation was aided by the proximity of other substrate molecules. In the zeolite, there is also the possibility that the rate of energy relaxation is site dependent. Perhaps $3^{\bullet+}$ is produced only from a small percentage of the adsorption sites in which the excited radical cation is metastable because of weaker coupling. The observation of $3^{\bullet+}$ from 2 as well as 1 in the zeolite implies either that the exothermicity of hole transfer is greater in zeolites than in freons, which is not likely, or that certain zeolite adsorption sites provide weaker coupling for energy transfer to the matrix than in freons.

Additional evidence that the nature of the zeolite interaction with the substrate radical cation influences this reaction is the fact that the observation of $3^{\bullet+}$ and $4^{\bullet+}$ depends on polarity. The percursor of $4^{\bullet+}$ is also thought to be an excited radical cation because the reverse Diels-Alder reaction is thermally forbidden. However, in this case, it must be assumed that the zeolite is capable of stabilizing the excited state up to approximately 200 K. We did not observe an excited state species by means of an EPR signal distinct from that of $2^{\bullet+}$. However, this does not rule out the existence of such a species, for the signal may have been hidden by the EPR signal from $2^{\bullet+}$.

Scheme I-3 depicts a possible mechanism involving $1^{\bullet+}$ and $2^{\bullet+}$ and the product radical cations. Some final remarks can be made regarding preliminary observation of the quadricyclane radical cation in polar zeolites at low temperature. In contrast to EPR spectra obtained at 4.2 K in freon matrices, which are broad and unresolved, our EPR spectra obtained after irradiation at 4.2 K of zeolites containing quadricyclane or norbornadiene show well-resolved structure, as shown in Figure 2. The spectra sharpen at higher temperatures and can be simulated (using the hyperfine coupling constants for the norbornadiene radical cation, 7.98 G(4H), 3.28 G(2H), 0.58 G(2H)) with linewidths of 0.3-0.4 G, compared to 5-6 G at 4.2 K.

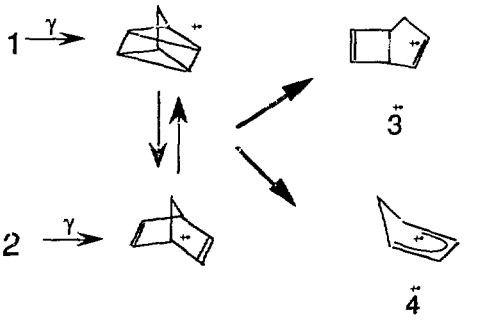

Scheme I-3

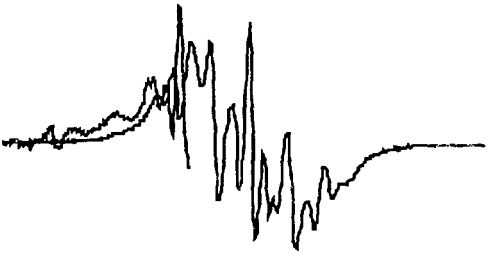

Figure 2. EPR spectrum observed at 4.2 K after irradiation at 4.2 K of norbornadiene in ZSM-5 zeolite. The broken line shows the low-field portion of the difference spectrum of quadricyclane and norbornadiene-loaded samples.

Notably, there are differences in the EPR spectra observed at 4.2 K in irradiated quadricyclane and norbornadiene samples that cannot be accounted for by line broadening. In quadricyclane-loaded samples, the full width of the spectrum is somewhat greater than in norbornadiene-loaded samples, and features are observable near the outer wings that are not present in the spectra from norbornadiene-loaded samples (Fig. I-2). These differences vanish when the quadricyclane-loaded samples are annealed above approximately 30 K, even after recooling to 4.2 K. The extra features become more prominent with increasing zeolite polarity.

The difference spectrum obtained from the 4.2 K spectra of the quadricyclane-loaded and norbornadiene-loaded samples shows similarities to the spectrum simulated from theoretical coupling constants for $1^{\bullet+}$. This is exciting evidence that we may have made the first observation of this very unstable radical cation, which has eluded observation by so many other researchers. We are pursuing this issue in still more polar ZSM-5 zeolites and hope to further enhance the presumed $1^{\bullet+}$ signal.

2. Silica Sol-gel Matrices for Radical Ion Studies *A. D. Trifunac, D. W. Werst*

Our EPR studies of radical cations in zeolites show the utility of such inorganic matrices for stabilizing and investigating reactive intermediates formed by high-energy processes. One shortcoming of zeolites is their opacity to light. This disadvantage precludes their use for most optical methods other than attenuated reflectance spectroscopy, which has limited applicability to zeolite samples. This year, we initiated the development of alternative silicate matrices with excellent transparency in the visible and ultraviolet.

Porous silica matrices were synthesized from organosilane precursors. For example, hydrolysis of alkoxysilanes leads to condensation reactions and the formation of a polymeric silica network, eqs. 2-3.

$$(RO)_3Si\text{-}OR + H_2O \rightarrow (RO)_3Si\text{-}OH + ROH \quad (2)$$

$$\text{-Si-OH} + \text{HO-Si-} \rightarrow \text{-Si-O-Si-} + H_2O \quad (3)$$

An alcohol solvent is used because the silane precursor is not miscible with water. The product after polymerization is a wet gel, containing water and solvent. If a monolithic, transparent product is desired, the gel is dried slowly to prevent cracking during solvent evolution, which is accompanied by considerable shrinking of the gel. All steps of gel preparation were carried out between room temperature and 60 °C.

An advantage of this sol-gel method for synthesizing inorganic matrices is that the low-temperature route allows organic modification of the material. The simplest way to introduce organic components is by doping organic molecules into the pores of the gel. We have synthesized silica sol-gels doped with a variety of aromatic compounds (e.g., p-terphenyl, naphthalene) by simply adding aromatic solutes to the alcohol solvent used in gel preparation. Absorption and fluorescence spectroscopy were used to verify that the aromatic species were incorporated into the sol-gel.

The sol-gel method also allows considerable variations to covalently modify the matrix with organic functional groups. For example, the use of alkyl- or aryltrialkoxysilane, $RSi(OR)_3$, precursors yields gels with silicon coordinated to three oxygen atoms and one R group. We have synthesized transparent sol-gels using $CH_3Si(OCH_3)_3$ and $C_6H_5Si(OC_2H_5)_3$ alone or diluted with the tetraalkoxysilane precursor. In this way, many properties of the matrix can be varied, such as the polarity of the pores. We have also prepared transparent sol-gels from mixtures of tetraalkoxysilanes and polyethylene glycol (MW_{av} = 200 g). The addition of the polyethylene glycol results in less shrinking and therefore a gel of lower density. This dramatic effect seems to indicate that the glycol molecules participate in condensation reactions and become covalently bonded to the network; that is, they are not merely trapped in the silica framework.

We have tested the silica sol-gels for resistance to optical damage when irradiated with ionizing radiation. The UV cutoff (~250 nm in the unirradiated material) shifted slightly to longer wavelengths after an absorbed dose of several megarad. The transparency of the sol-gels throughout the rest of the spectrum, to 900 nm, was unaffected. It is important that the matrix used to study intermediates generated by ionizing radiation not give rise to interfering absorbances induced by the radiation.

Future experiments will investigate the formation of trapped radical ions in sol-gel matrices. Preliminary studies of transient radioluminescence from pulse-irradiated sol-gels doped with aromatic molecules indicate that the yield of exited states of the substrate molecules from ion recombination is low in the unmodified SiO_2 material. In contrast, sol-gels modified with polyethylene glycol give rise to a strong delayed fluorescence component that is due to ion

recombination. The glycol-modified sol-gels are promising media for carrying out fluorescence-detected magnetic resonance (FDMR) studies of radical cations.

A separate effort was begun to develop sol-gel matrices for EPR studies of matrix-isolated radical ions. The synthetic methods used are similar, except that monolithic, transparent samples are not needed. In fact, small particles are more easily introduced into the EPR spectrometer and low-temperature cryostat. Powdered or granulated sol-gels are obtained by mechanical grinding of large particles or, in some cases, by spontaneous cracking of the gel during rapid drying. Porous silica sol-gels are expected to have some properties in common with other inorganic matrices, such as zeolites, used for studying trapped radical ions. Obviously, the amorphous sol-gel matrix differs from zeolites in that it does not have a well-defined pore size. Nevertheless, the pore size and distribution can be controlled to a degree by preparation conditions. This, together with organic modification of the sol-gels, offers a variety of ways to modify the physical environment of radical cations and study the influence of such environmental changes on their behavior.

One encouraging test of the ability of the silica sol-gels to stabilize radical cation species involved the substrate molecule, N,N,N',N'-tetramethyl-p-phenylenediamine (TMPD). TMPD is very easily oxidized, and, in the polar reaction mixture used to synthesize the TMPD-doped sol-gel, the TMPD radical cation formed without irradiation. $TMPD^{\bullet+}$ remained stable in the dried sol-gel even at room temperature. This was verified by both EPR and optical spectroscopy.

3. Ion Recombination in Solids

A. D. Trifunac, D. W. Werst, I. A. Shkrob

A combination of experiments and theoretical modeling was carried out to investigate the mechanism of charge recombination in the solid state at low temperatures. The main question is, in the absence of molecular diffusion, how does rapid radical ion recombination proceed? The simplest mechanism is back electron transfer via single-step tunneling. Other mechanisms must invoke some mode of charge migration without molecular displacement, such as resonant charge transfer or thermal detrapping of electrons. Such hypotheses may be applicable in some systems in which radical ion recombination occurs on the submicrosecond time scale.

The experimental method used to investigate ion recombination in low-temperature solids was time-resolved FDMR. Fluorescence-detected magnetic resonance detects electron spin resonance in the geminate radical ion pairs produced by radiolysis that undergo spin-selective electron transfer. Because the yield of radioluminescence upon ion recombination depends on the multiplicity of the product excited state, and thus on the spin phasing in the pairs, spin transitions in the radical ion pairs are detected as an increase or decrease in the fluorescence intensity. The amplitude of the FDMR signal is directly related to the lifetime of the pairs (i.e., recombination rate) and rate of spin mixing induced by an applied microwave field.

The rate of single-step electron tunneling depends exponentially on distance, $K(r) = K_0\exp(-r/\lambda)$. In order to observe an FDMR signal, the ion-pair lifetimes must be on the timescale of the spin dynamics within the pairs. Very fast (<10 ns) recombination allows insufficient time to perturb the spin states of the reacting radical ions with the applied microwave field. In the event that recombination is very slow (many microseconds), spin relaxation begins to erase all memory of the original spin phasing of the pairs, and no FDMR signal will be observed. In the rigid solid, where pair-separation distances become fixed, only a fraction of the radical ion pairs, representing a narrow slice of the ion-pair-separation distribution, can be FDMR active according to a single-step electron tunneling model.

One prediction of the single-step tunneling mechanism is that there should exist an optimal separation distance for FDMR; that is, the FDMR amplitude should have a maximum value for some separation distance and decrease for smaller or larger distances. However, the experimentally obtained distribution of ion-pair-separation distances is difficult to control. The distribution will depend on certain variables under experimental control, however, such as scavenger concentration or the molecular structure of the solvent. A novel approach used in our work was to artificially narrow the separation-distance distribution by forming bridged radical ion pairs in detergent molecules organized in micelles in aqueous media.

a. FDMR in Frozen Aqueous Micellar Solutions

FDMR experiments were carried out in the temperature range 30-80 K in aqueous solutions of 5-10

wt.% polyoxyethylene alkylphenols, known as Triton X detergents. The molecules comprising the Triton series have an aromatic head group (1,1,3,3-tetramethylbutylphenoxy) and a polyoxyethylene tail. The polydisperse detergents used in our study had average numbers of oxyethylene units equal to 5 to 40. The proposed mechanism of FDMR in these frozen micellar solutions is depicted in Figure 3.

Interaction of fast electrons with the micelles produces positive holes localized somewhere along a polyoxyethylene tail and ejected electrons. Some of the electrons attach to the aromatic head group of the detergent molecule on which its parent hole resides; that is, a bridged geminate ion pair is produced. Nonbridged pairs are also produced, but our results indicate that the recombination times of these pairs are less optimal for FDMR detection. Therefore, bridged ion pairs that undergo intramolecular recombination account for the vast majority of FDMR active pairs in the micellar solutions.

Scavenging experiments and tests using model compounds all support the above mechanism. In every case, intermolecular electron transfer generated a smaller FDMR signal than electron transfer in bridged pairs. This was found in homogeneous alcohol solutions (frozen) of the detergent molecules as well as the aqueous micellar solutions. Figure I-4 shows the dependence of the FDMR amplitude on the number of oxyethylene units. It was maximum for $n = 9.5$ and decreased for shorter or longer tails. This is the functional dependence that is expected if the ion-pair-separation distribution is shifted to larger separation distances for longer polyoxyethylene tails.

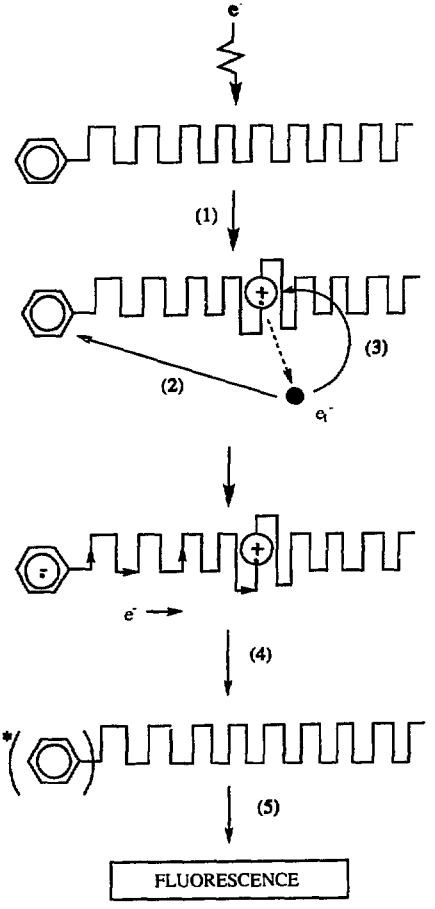

Figure 3. Reaction steps that lead to the FDMR signal in aqueous micellar solutions.

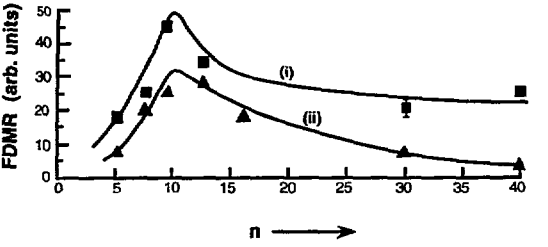

Figure 4. Dependence of the FDMR amplitude in micellar solutions on the number of oxyethylene units, n, in Triton X detergent molecules in (i) aqueous and (ii) 2-propanol solutions (at ~10 K).

b. FDMR in Low-Temperature Organic Solids: Theory and Experiment

The behavior of FDMR in frozen organic solids is more complicated than in the artificially confined pairs generated in micelles. The distribution of separation distances between geminate pairs of ions is broader, and less is known about these distributions for solids than for liquids. If one assumes a correlation between electron thermalization distances in liquids and in solids, then one can rank different organic compounds according to the relative scale of electron-transfer radii involved in ion recombination. In fact, the FDMR intensities measured in a large number of frozen alcohols, ethers, olefins, alkanes, etc., correlate approximately with known electron thermalization

distances in the respective liquids. This finding suggests that electron tunneling is a primary mode of ion recombination in the solid state on the submicrosecond timescale that is probed by FDMR.

As an aid in gleaning more information from the behavior (kinetics, microwave power dependence, concentration dependence, etc.) of the FDMR signal in solids, a theoretical framework based on a single-step electron-tunneling mechanism and the Liouville approach for the description of spin and reaction dynamics in geminate pairs was developed. Although the theoretical model reproduces many qualitative features of the experimental data, such as t^{-1} decay kinetics, narrow radial distribution of FDMR active pairs, and spin coherence transfer, its quantitative predictions seem to underestimate the degree of charge mobility. For this reason, two modifications to the single-step electron-tunneling model are being considered. These are (1) resonant charge transfer involving the solvent holes and (2) the existence of electrons in weakly bound states. The latter would increase the estimate for the tunneling radii in reactions of negative charges.

4. Multiphoton Processes in Liquids

M. C. Sauer, Jr., A. Liu, K. H. Schmidt, A. D. Trifunac

Alkane liquids and solutions of aromatic compounds are known to be ionized by intense UV light from sources such as excimer lasers. In cyclohexane and trans-decalin, positive ions with anomalously high mobility (HM_+) have been observed by such photoionization. High-mobility cations have also been observed in the radiolysis of these and other saturated hydrocarbons with C_6 rings (cis-decalin, methylcyclohexane). Investigations aimed at identifying HM_+ have been a continuing subject of research in our laboratories, and evidence that suggests that HM_+ is the protonated solvent molecule has been examined.

Recent observations via transient optical absorption spectrophotometry in our laboratories have shown that the quantum yield of aromatic radical cations created by such laser photoionization decreases with increasing light intensity. The conclusion was reached that absorption of a photon by the aromatic radical cation promotes a reaction of the radical cation with the solvent. On the basis of the results of product analysis and effects of intensity on the absorbance observed due to the aromatic radical cation, the reaction was concluded to be proton transfer. The general mechanism proposed for solutions of aromatic molecules in alkanes (or alcohols), where ArH and RH represent the aromatic molecule and the alkane solvent, respectively, is as follows.

$$ArH + h\nu \longrightarrow {}^1ArH \quad (4)$$

$${}^1ArH + h\nu \longrightarrow ArH^{\bullet+} + e^- \quad (5)$$

$$ArH^{\bullet+} + h\nu \longrightarrow ArH^{\bullet+*} \quad (6)$$

$$ArH^{\bullet+*} + RH \longrightarrow Ar^{\bullet} + RH_2^+ \quad (7)$$

This mechanism, combined with previous observations of HM_+ in cyclohexane and trans-decalin, indicates that HM_+ is the protonated solvent, RH_2^+. Observations in radiolysis studies and subpicosecond two-photon ionization studies that alkane radical cations have short lifetimes (due to reactions other than charge recombination), and the chemical stability of ground state $ArH^{\bullet+}$ with respect to reaction with the alkane solvent, are consistent with transfer of charge to the solvent via ion-molecule reaction 7.

For neat alkanes, the same evidence supports the production of protonated solvent by reaction 8.

$$RH^{\bullet+} + RH \longrightarrow R^{\bullet} + RH_2^+ \quad (8)$$

Using transient photoconductivity measurements, we have carried out a detailed reexamination of the wavelength and intensity dependence of the yield of HM_+ in both neat solvents and solutions of aromatic molecules to determine whether such observations are consistent with this mechanism. The general procedure was to measure the yields of free electrons and HM_+ at 248 and 308 nm as a function of laser pulse intensity for neat solvents and for solutions containing aromatic compounds. In neat cyclohexane and trans-decalin, the yields of electron and HM_+ have the same intensity dependence; for ionization of these two alkanes, two photons are required at 248 nm, and three photons at 308 nm. In solutions containing aromatic solutes, where the major fraction of the light absorption is by the solute, yields of free electrons and HM_+ are markedly higher. At both 248 and 308 nm, the intensity dependences indicate that two photons are required for ionization, but that three photons are required to create HM_+. This is consistent with the explanation, based on our product analysis studies, that the aromatic excited state reached with one photon is ionized by a second photon. The radical cation then absorbs a third photon and reacts with the solvent to

form HM_+. The observed decrease in the quantum yield of the anthracene radical cation in 2-propanol with increasing intensity can be explained similarly. In the neat solvents, the production of HM_+ can be ascribed to the reaction of the radical cation of the solvent, produced by simultaneous two- or three-photon absorption, with a solvent molecule, which is consistent with a body of results bearing on the fate of alkane radical cations in radiolysis.

a. Results with Neat Solvents

Figures I-5 and I-6 show representative results on neat solvents. Three different conductivity signals were measured: (1) the signal at 50 ns after the beginning of the laser pulse in neat liquids or solutions degassed with Ar, primarily due to the electron (e^-) and the high-mobility positive ion (HM_+); (2) the signal at 50 ns after the beginning of the laser pulse in neat liquids or solutions degassed with SF_6, primarily due to HM_+, but contributed to by normal-mobility ions; and (3) the signal due to scavenged free ions. The conductivity signal (3) is due to the ions that have escaped geminate recombination and is measured after scavenging of electrons by SF_6 and conversion of HM_+ to a normal mobility cation, but before homogeneous recombination begins. These signals were determined from measurements of conductivity vs. time.

In Figs. I-5 and I-6, the experimental values of signals (1) and (3) are plotted without alteration. To obtain HM_+ vs. light intensity, signal (3) was subtracted from signal (2). This is an approximation because part of the signal at 50 ns is due to geminate ions other than HM_+, and the free ion signal due to ions other than HM_+ is smaller at 50 ns than signal (3). The resulting error is negligible for the neat solvents, but is expected to cause the signal labeled HM_+ to be too large for solutions containing aromatic solutes.

The conductivity signals were divided by the incident light intensity and plotted vs. incident light intensity on a log-log scale. For a two-photon process, a line of slope unity is expected (as is observed) for such a plot if the fraction of the light absorbed is negligible. The experimental results are compared with a curve calculated by the finite element analysis method, which is not described in detail here. Briefly, in this calculation, parameters for two- or three-photon ionization (a_2 and a_3) are chosen by trial and error to match the electron conductivities observed at low

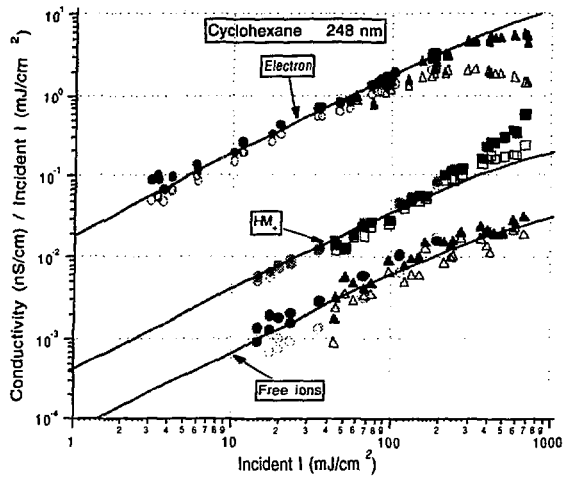

Figure 5. Intensity dependence of ionization in cyclohexane at 248 nm. The upper set of points is for a solution degassed by bubbling with argon, and the middle and lower sets with SF_6. The various symbols represent different conditions of laser operation or treatment of the data. The curves are calculated as described in the text, for a two-photon ionization process.

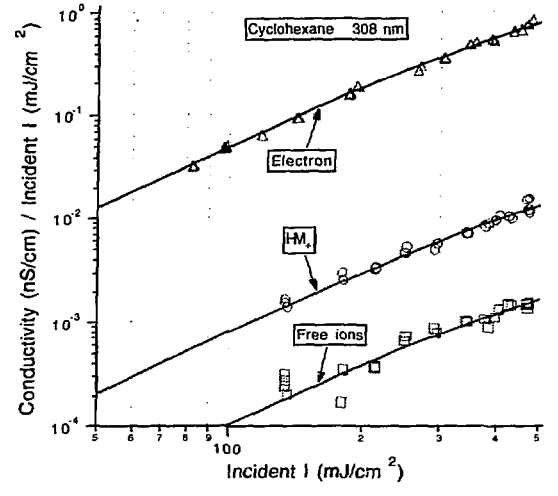

Figure 6. Intensity dependence of ionization in cyclohexane at 308 nm. The upper set of points is for a solution degassed by bubbling with argon, and the middle and lower sets with SF_6. For the upper and middle sets, the signals are at 50 ns after the beginning of the pulse; decay due to recombination is not appreciable because of the low concentration of ions. The free ions (lower set) were measured at 2 μs. The curves are calculated as described in the text, for a three-photon ionization process.

intensity, and the fraction of escaped ions (f_{fi}) is adjusted until the measured power absorption is matched. The parameters derived in this manner for ionization of the neat solvents are given in Table 1. The same calculated curve, normalized to account for the different mobilities, is reasonably consistent with all three conductivity signals in Figure 5, which indicates that every ionization results in a constant ratio of HM_+ to electron, independent of intensity.

Table 1. Coefficients for production of free ions and the probabilities, f_{fi}, for separation into free ions in neat liquids.[a]

liquid	wave-length (nm)	a_2	a_3	f_{fi}[b]
cyclohexane	248	1.9×10^{-20}	0	0.0060
"	308	0	1.3×10^{-31}	0.0030
trans-decalin	248	1.4×10^{-20}	0	0.010
"	308	0	1.3×10^{-30}	0.020

[a]To obtain the rate of production of free ions during a laser pulse in moles liter^{-1} sec^{-1}, a_2 is multiplied by the square, and a_3 by the cube, of the intensity in mJ cm^{-2} s^{-1}. The total rate of ionization is greater than this by $1/f_{fi}$.

[b]The values of f_{fi} given in this table are for a field strength of 7.1 kV cm^{-1}. The values of f_{fi} are therefore higher than the separation probabilities at zero field strength by factors of 1.41 for cyclohexane and 1.36 for trans-decalin.

For cyclohexane at 308 nm (Figure 6), the slope of the plot is nearly 2 and therefore consistent with a three-photon ionization. This is expected, because two photons have insufficient energy to ionize cyclohexane.

The results on neat solvents can be described by reactions 9-11.

$$RH + 2hv \text{ or } 3hv \longrightarrow RH^{\cdot+*} + e^- \quad (9)$$

$$RH^{\cdot+*} + RH \longrightarrow R\cdot + RH_2^+ \quad (10)$$

$$RH^{\cdot+*} \longrightarrow H_2 + \text{olefin}^{\cdot+} \quad (11)$$

RH_2^+ is the high-mobility cation, HM_+. The results of other studies establish that reaction 10 occurs, although excitation may not be required, in which case reaction 10 becomes identical with reaction 8. The results of the present study are completely consistent with reaction 10, and this is supported by the preponderance of relevant radiolysis studies.

The ratio of HM_+ signal to electron signal is of interest because, if we accept the literature values of the mobilities, it is a measure of the fraction, f_{HM+}, of the ionization events that produce HM_+. Values of f_{HM+} of 0.35 for neat cyclohexane and 0.6 for neat trans-decalin (for both 248 and 308 nm) were obtained by analysis of the results.

The value of f_{HM+} is less than unity, suggesting that not every escaped positive ion is HM_+. This conclusion depends on the accuracy of the mobility values. The radiolysis/microwave-conductivity method by which the mobilities of HM_+ in cyclohexane and trans-decalin were determined would result in a low value of the mobility if not all of the positive ions produced by radiolysis were HM_+. If the true values of μ_{HM+} are higher than reported, the values we would obtain for f_{HM+} would be even smaller. Therefore, we must conclude that at least 65% and 40% of the escaped positive ions are not HM_+ for cyclohexane and trans-decalin, respectively.

A possible reason for $[HM_+]/[e^-]$ values less than unity is that HM_+ is formed by proton transfer or charge transfer from an excited cyclohexane radical cation that also decays by a competing process, for example, reaction 11. Evidence of such reactions has been obtained for alkane liquids and solutions even under conditions where $RH^{\cdot+}$ contains little, if any, excitation.

b. Results with Aromatic Solutes

The addition to cyclohexane of a small concentration of a solute such as anthracene or pyrene, which absorbs light significantly at the laser wavelength, causes a marked increase in the yield of ionization. The yield of HM_+ is likewise enhanced.

Figure I-7 shows the intensity dependence at 248 nm of the electron yield (Ar-saturated solutions) and the HM_+ yield (SF_6-saturated solutions) obtained for 2×10^{-6} M anthracene in cyclohexane. These results strongly support the three-photon nature of the production of HM_+ in this system. This can be seen qualitatively by noting that at low intensities the slope of the curve for the electron or the free ions is close to the value of unity expected for a two-photon process, whereas the slope for HM_+ is near to two, the value expected for a three-photon process. The curves through the experimental data in Figure 7 were calculated by using the method described briefly in the following.

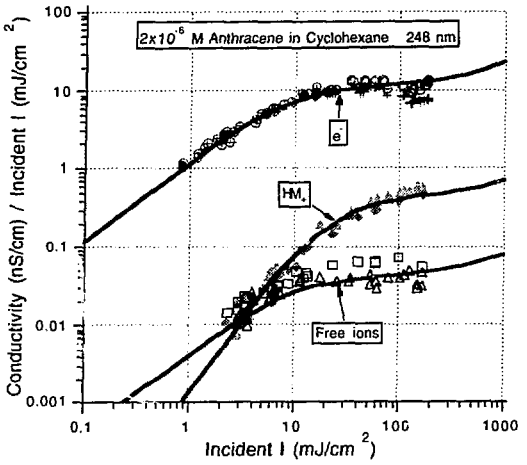

Figure 7. Intensity dependence of ionization in 2×10^{-6} M anthracene in cyclohexane at 248 nm. The upper set of points is for a solution degassed by bubbling with argon, and the middle and lower set with SF_6 (triangles) or CO_2 (diamonds or squares). In the upper set, the circles are obtained by correcting the pluses for ion recombination. The curves are calculated as indicated in the text; mobility values from the literature were used except that the mobility of HM_+ had to be increased by 20% to obtain a match with the experimental points.

Two-photon ionization of the solvent was included in the calculations by using the parameters derived from the results on neat cyclohexane and given in Table 1. Absorption of light by the ground and excited states of anthracene and the radical cation of anthracene was calculated using the absorption coefficients given in Table 2. The yield of free ions is determined by the values chosen for these absorption coefficients and the quantum yield for separation into free ions, Φ_{fi}. The yield of HM_+ depends on Φ_{fi} and the absorption coefficient chosen for the aromatic radical cation. Therefore, the proposed mechanism, where absorption of a 248 nm photon by the anthracene radical cation leads to formation of HM_+ in cyclohexane, is well substantiated by the agreement of the calculated and experimental results for the concentrations of ions and the calculated and experimental power absorptions.

Similar results (not shown) were obtained for 5×10^{-6} M pyrene in cyclohexane for 308 nm excitation. The results show that the yield of HM_+ increases more rapidly than the yield of ionization, just as was observed for 248 nm excitation. Again, a three-photon mechanism for HM_+ formation is indicated.

The ratios of HM_+ conductivity to electron conductivity at 248 nm obtained from Figure 7 and the analogous results at 308 nm show that the relative HM_+ yield is much smaller for the 308 nm photoionization. An analysis of the conductivity ratios at 100 mJ cm^{-2} shows that values of f_{HM+} of 0.9 and 0.12 can explain the 248 and 308 nm results, respectively. The low value at 308 nm appears to be primarily due to incomplete conversion of $Py^{\cdot+}$ (the pyrene radical cation) to HM_+, because of the low

Table 2. Parameters in experiments and calculations on cyclohexane and 2-propanol solutions.[a]

parameter[b]	2 μM A/chex	5 μM Py/chex	2 μM A/2-prop
known quantities[c]:			
laser wavelength (nm)	248	308	248
$\varepsilon_{ground\ state}$ ($M^{-1}\ cm^{-1}$)	1.2×10^5	1.14×10^4	1.2×10^5
$k_{singlet \rightarrow ground\ state}$ (s^{-1})	5.0×10^7	1.44×10^6	5.0×10^7
$k_{singlet \rightarrow triplet\ state}$ (s^{-1})	9.2×10^7	6.5×10^5	9.2×10^7
derived quantities:			
$\varepsilon_{singlet\ state}$ ($M^{-1}\ cm^{-1}$)[d]	3.0×10^4	4.6×10^3	3.6×10^4
$\varepsilon_{triplet\ state}$ ($M^{-1}\ cm^{-1}$)[d]	3.0×10^4	4.6×10^3	3.6×10^4
$\varepsilon_{radical\ cation}$ ($M^{-1}\ cm^{-1}$)[d]	2.0×10^4	1.26×10^3	1.3×10^4
Φ_{fi}	2.2×10^{-3}	9.0×10^{-4}	3.2×10^{-2}
$\Phi_{radical\ cation \rightarrow HM+}$	1.0	1.0	1.0

[a]A, Py, chex, and 2-prop represent anthracene, pyrene, cyclohexane, and 2-propanol, respectively.
[b]The designations for ε's, Φ's, and k's refer to the aromatic solute, except for Φ_{fi}. The ε's are at the laser wavelength.
[c]The values of ε and k given are from the literature. Excimer formation in pyrene solutions is known to occur, but would not be significant for the concentrations used here on the time scale of interest.
[d]At the laser wavelength.

absorptivity of $Py^{\cdot+}$ at 308 nm. At 248 nm, a much larger fraction of $An^{\cdot+}$ (the anthracene radical cation) is converted to HM_+; this is evident from inspection of the results for HM_+ in Figure 7, where leveling off of the HM_+ signal at higher intensities is seen. The large difference in the 248 nm values of f_{HM+} for neat cyclohexane and anthracene in cyclohexane shows that the creation of HM_+ when $An^{\cdot+}$ absorbs a photon is considerably more efficient than formation of HM_+ in the simultaneous two-photon ionization of cyclohexane. In other words, in the latter process, the formation of some other positive ion must account for a large fraction of the ionizations.

Figure I-8 uses results from an earlier study of 248 nm laser ionization of anthracene in 2-propanol, and shows that those results can also be explained by the same model as used for the alkane solutions. The solid curves shown in Figure 8 were obtained using the parameters given in Table 2.

The intensity effects (which indicate the "bleaching" of the ground state aromatic radical cation) show that HM_+ is formed via an excited state of the aromatic radical cation, and are completely consistent with the formation of the high-mobility species by reactions 4-7. Reaction 7 may involve charge transfer or proton transfer on the basis of the observed intensity effects. Evidence that HM_+ is protonated cyclohexane comes from product analysis studies, where the conclusion was reached that the aryl radical was formed, based on the increase in products resulting from cyclohexyl radicals when anthracene was present as well as from the observation of corresponding amounts of $C_{14}D_9H$ when perdeuterated anthracene

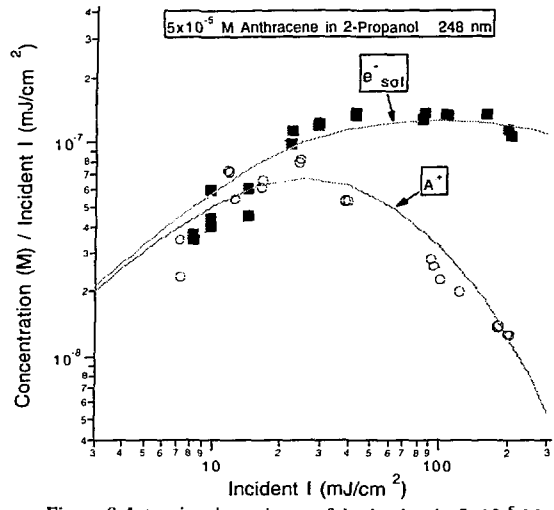

Figure 8. Intensity dependence of ionization in 5×10^{-5} M anthracene in 2-propanol at 248 nm. The upper set of points is for a solution degassed by bubbling with argon, and the lower set with SF_6. The concentrations were obtained from the e^-_{sol} absorption at 840 nm and the anthracene radical cation absorption at 720 nm for the upper and lower sets, respectively. The curves are calculated as described in the text.

was used (the aryl radical reacted mainly by abstraction of H from cyclohexane). This assignment is consistent with radiolysis results bearing on proton transfer referred to earlier, as well as with a number of magnetic resonance studies that indicate that radical cations of alkanes undergo reaction 4, and do so by proton transfer rather than hydrogen atom abstraction.

B. The Role of Solvent in Chemical Reactivity

A. D. Trifunac, D. M. Bartels, C. D. Jonah, Y. Lin, K. H. Schmidt, S. Mezyk, E. Roduner, P. W. Percival

1. H- and D-Atom Encounters with O_2 in Water *D. M. Bartels*

Several recent studies from this laboratory have taken advantage of electron pulse radiolysis combined with pulsed, time-domain EPR detection to measure reaction rates of H and D atoms in water. Comparison of H reaction rates in water with the gas-phase values is a promising venue in the fundamental study of solvent effects in chemical reactions. The technique, based on the attenuation of free induction decays (FIDs) in the presence of radical scavenger, is superior to previous EPR methods in that the destruction of spin-phase coherence by H-atom scavenger follows simple pseudo-first-order kinetics. This bypasses the problem of very complicated kinetics caused by the chemically induced dynamic electron polarization (CIDEP) phenomenon in the longitudinal magnetization. EPR detection of H atoms is advantageous in terms of its great specificity; the doublet spectrum of ca. 510 gauss splitting is impossible to mistake for any other radical. Detection of the D-atom triplet is just as specific, and in a recent publication we demonstrated that H/D isotope effects can be

determined by simultaneous measurement of the H and D reaction rates in a 90% D_2O/10% H_2O mixture.

It has been argued, based on the similarity of muonium and hydrogen atom rate constants in the diffusion-limited regime, that there is essentially no isotope effect in the diffusion of H or Mu (or D) atoms in light water. Measurement of absolute H and D diffusion coefficients in H_2O and D_2O separately has found roughly a square-root of mass difference, but this experiment cannot differentiate atomic mass and solvent isotope effects. The present study was inspired as an attempt to clarify this issue by simultaneous measurement of diffusion-limited H and D reaction rates in the same H_2O/D_2O mixture, to avoid any possible effects of viscosity or density differences between light and heavy water. Molecular oxygen was chosen as a reaction partner because it is easy to replenish its concentration in a recirculating flow system by continuous bubbling. Previous reports of the H + O_2 reaction rate suggested that the reaction to form HO_2 is not actually diffusion limited, but nearly so. It was not anticipated that this would matter in the present context because either chemical reaction or spin exchange between the paramagnetic H and O_2 species will cause loss of phase coherence in the FID attenuation experiment.

H and D atoms were generated within an EPR cavity by pulse radiolysis of aqueous solutions with 5-25 ns pulses of 3 MeV electrons from a Van de Graaff accelerator. Immediately following creation of the radicals, a 30 ns $\pi/2$ microwave pulse is applied to the EPR cavity. After a ca. 130 ns receiver "dead time", FIDs of the H atoms can be observed, as shown in Figure 9. One thousand shots were averaged to produce the signal-to-noise ratio illustrated. The signals are well described as a simple damped cosine, and the information of interest is contained in the reduction of damping time constant with scavenger concentration (Figure 9). The effective T_2 will be given by

$$1/T_2(\text{eff}) = 1/T_2^{\circ} + k_S[S] + \sum_i k_{ex}^i[R_i] \qquad (12)$$

where $1/T_2^{\circ}$ is the (small) natural dephasing rate, $k_S[S]$ is the scavenging rate of interest, and $\sum k_{ex}^i[R_i]$ represents the contribution of all spin exchange and reaction due to second-order radical-radical encounters. In general, the free radical concentrations are sufficiently low that the latter term is virtually constant, if not negligible, on the 5 μs time scale of the FID. Rate constants are easily determined by incremental addition of scavenger to produce a linear plot of damping rate vs. scavenger concentration.

Results for all experiments in H_2O are plotted in Arrhenius form in Figure 10. The rate constants are similar to but slightly larger than reaction rates reported by other workers, as to be expected for a spin exchange process. Results for both H and D encounters with O_2 in 90% D_2O/10% H_2O are presented in Figure 11. The rate constant for D is consistently 5-10% lower than the rate for H. The rate constant for the H + O_2 dephasing in 90% D_2O is consistently less than the rate in pure H_2O, and seems to have a lower activation energy. However, care should be taken not to overinterpret this comparison given the available S/N ratio.

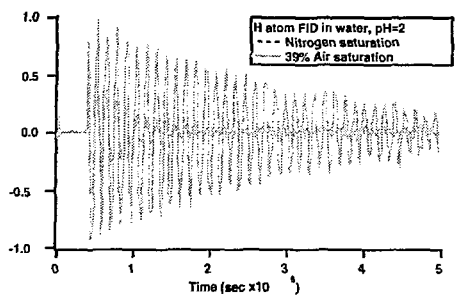

Figure 9. Typical FIDs of the H-atom low-field ($m_I = +1/2$) line immediately following pulse radiolysis of pH 2 aqueous solution. The FID is attenuated in the partially air-saturated solution by the presence of O_2.

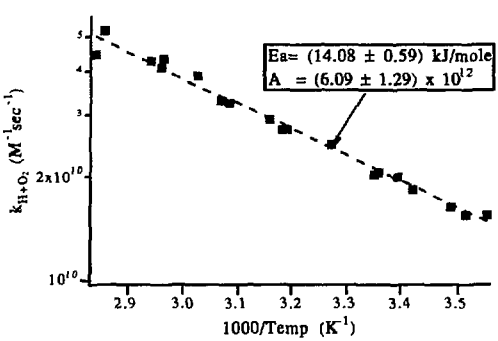

Figure 10. Rate constants for bimolecular dephasing of H atoms by O_2 in H_2O.

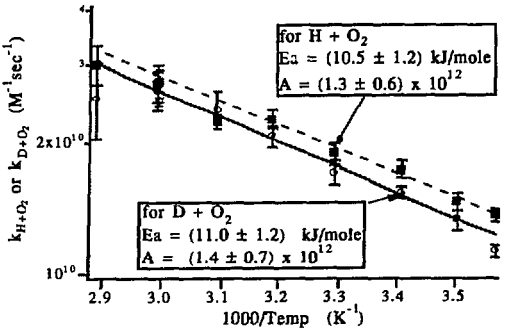

Figure 11. Dephasing rate constants for both H and D atoms in 90% D_2O/10% H_2O.

It has been asserted, based on the similarity of many H atom and Mu reaction rates in the diffusion limit, that there is virtually no difference in their diffusion rates. The factor of nine difference in mass should appear as a three times larger reaction rate for Mu if the system behaved like a dilute gas. A roughly $\sqrt{2}$ difference between H diffusion in H_2O and D diffusion in D_2O was also reported, but it was suggested that the primary mass effect might be the librational frequency of the water molecules, rather than the mass of the diffusing atoms. We are now in a position to clarify this issue. First, given the comparison of H and D spin dephasing in Figure 11, there definitely is an atomic mass effect on the diffusion rates in water. In water of a given isotopic composition, the lighter atom moves faster. However, the effect is significantly less than a classical square-root-of-mass dependence. Secondly, there is also a difference between the dephasing rates for H atoms in H_2O and in 90% D_2O water, and an apparent difference in the activation energies that does not parallel T/η. The great importance of water librational motions in controlling the diffusion should not be discounted, but the diffusion coefficient is complicated by several simultaneous effects. There is clearly room for better theoretical understanding of these light-molecule diffusion processes in water, and more high-precision measurements of diffusion rates over a wide temperature range. The issue is far from esoteric, as many isotopic tracer techniques used in geology and oceanography depend critically on gas-transport properties in water.

2. Reaction of H atoms with I^- and Br^-

D. M. Bartels, S. Mezyk

The study of the radiation-induced chemistry of iodine-containing species in the aqueous phase has been stimulated by the recognized safety hazard of radioactive iodine release following a nuclear reactor accident. There now exists a significant body of information on the reactions of iodo-substituted species with a variety of free radicals in aqueous solution. However, the paucity of data for H-atom reactions with even the simplest of these species has meant that models for predicting the volatility of radioactive iodine under accident conditions are incomplete. Furthermore, even when such data are available, as for the H-atom reaction with I^-, the large scatter in the reported rate constants has made their inclusion in these modeling schemes essentially futile. To begin to rectify this situation, we have undertaken measurement of rate constants for the reaction of H atoms with I^- and Br^-. Our FID attenuation method is particularly advantageous for this purpose because of the simple pseudo-first-order scavenging kinetics generally obtained. Important insight into the nature of the products is also gained from H-atom spin exchange and CIDEP in the presence of the halide ions.

The FID attenuation experiment was carried out as described above. Hydrogen-atom longitudinal magnetization was also recorded as a function of time after the radiolysis pulse for several different scavenger concentrations, by scanning the microwave pulse delay relative to the radiolysis pulse, and integrating the first 100 ns of the FID signal in a gated integrator.

Rate constants for the reaction of H + I^- were measured by FID attenuation at several temperatures in the range 10-57 °C, and results are plotted in Arrhenius form in Figure 12. At 25 °C, the rate constant (extrapolated to zero dose) is $2.8 \pm 0.4 \times 10^8$ M^{-1} sec^{-1}. The reaction rate is found to be remarkably insensitive to the temperature, with fitted activation energy of only 1.8 ± 4.6 kJ/mole. Rate constants for the reaction of H + Br^- were also measured over the 10-58 °C temperature range, and the results are also included in Figure 12. At 25 °C the rate constant is $1.7 \pm 0.3 \times 10^6$ M^{-1} sec^{-1}. As in the iodide case, the reaction of H with Br^- seems to have only a small activation energy of 6.3 ± 6.2 kJ/mole.

The CIDEP of the H atom in the presence of the halide ions was also recorded as a function of time, and the results were quite curious in light of the rate

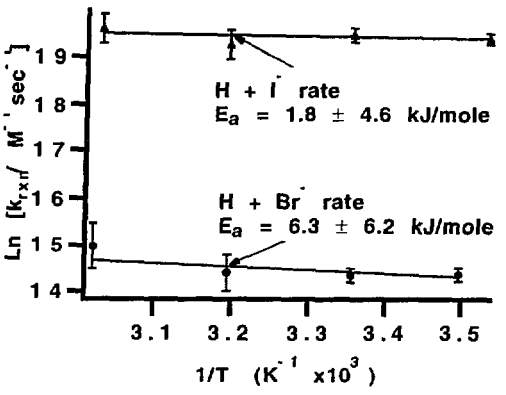

Figure 12. Arrhenius plots of Ln[k_{rxn}] vs. 1/T for the reaction of H atoms with I^- and Br^- in aqueous solution.

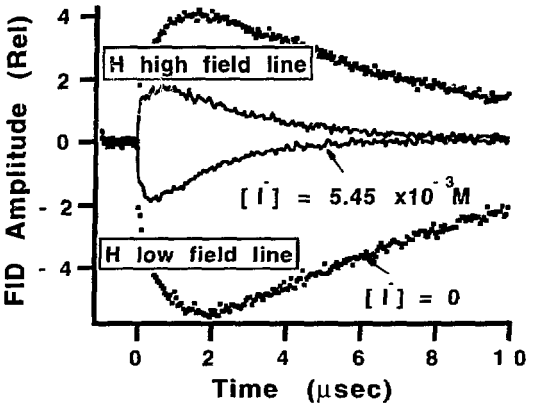

Figure 13. Effect of I^- on H-atom CIDEP in pH 3 perchloric acid solution at 25 °C following a 25 ns radiolysis pulse. In the presence of 5.45×10^{-3} M iodide, the chemical lifetime of the H atoms should be only 680 ns, but magnetization persists beyond 10 μs.

constants determined by FID attenuation. In Figure 13 we show the H-atom magnetization in the presence of 5.45×10^{-3} M iodide. The decay of H magnetization is anomalously slow, given the expected 660 ns chemical lifetime, and the measured FID decay time of 480 ns. Observable H-atom magnetization persists beyond 10 μs. Similar behavior is found in the Br^- scavenging systems. Qualitatively similar results, where the magnetization decay time lagged the calculated chemical decay by factors of two to four, were obtained in the presence of both I^- and Br^- in solutions of pH 1, 2, and 3. The same phenomenon was also found in iodide-containing solutions at neutral pH. No indication was found that the FID attenuation rate might be a function of pH.

The H-atom magnetization decay may slightly lag the chemical decay if polarization is generated in subsequent H + product free radical cross recombinations. However, it is unreasonable to expect this behavior when the product is HBr^- or HI^-. Small linear free radicals tend to have very fast spin relaxation times due to the spin-rotation coupling mechanism. The presence of the heavy atom in the HX^- molecules should enhance the spin relaxation even further, to the point that spin coherence does not persist between reencounters of HX^- and H radicals. In this limit, CIDEP will not be generated. Even if H-atom CIDEP could be efficiently generated in such encounters, the chemical conversion of H to the product radical will ensure that the H magnetization decay only slightly lags (10-20%) the chemical decay. The CIDEP decay times observed in the halide solutions differ dramatically from the rate constants deduced in the FID attenuation experiments.

We suggest that this anomalous CIDEP result in the halide scavenging systems is consistent with an equilibrium $H + X^- \rightleftharpoons HX^-$, which is established on a microsecond time scale. In this case, the FID decay time will be controlled primarily by loss of spin coherence in the forward reaction, but additional CIDEP can be generated by self-recombination of the residual H atoms. Back reaction rates on the order of 10^6 sec^{-1} would be required to maintain a sufficient H-atom concentration to qualitatively explain the CIDEP results.

In their pulse radiolysis/transient absorption study of the production of I_2^- in iodide-containing acid solutions, Elliot et al. demonstrated that the observed formation kinetics were consistent with the following mechanism:

$$H + I^- \rightleftharpoons HI^- \qquad (13)$$

$$HI^- + I^- \rightleftharpoons HI_2^= \qquad (14)$$

$$HI_2^= + (H^+)_{aq} \rightarrow H_2 + I_2^- \qquad (15)$$

Under the conditions of their experiments (large I^-, $(H^+)_{aq}$ concentrations), reaction 15 was shown to be rate-limiting ($k_8 = 2.3 \pm 0.4 \times 10^7$ M^{-1} sec^{-1}), with the H atoms, HI^-, and $HI_2^=$ reaching a preequilibrium on a submicrosecond time scale ($K_7 = 0.82 \pm 0.13$ M^{-1}). They considered only the forward reaction of 13, whose rate they deduced must be greater than or

equal to about 4×10^8 M^{-1} sec^{-1}, in good agreement with our FID attenuation measurement (2.7×10^8 M^{-1} sec^{-1}). It appears that the data collected by Elliot et al. demands $K_{19} > 25$ M^{-1}. Values of k_{-19} on the order of several times 10^6 sec^{-1}, as required to explain our CIDEP results, are perfectly compatible with the mechanism shown above.

The discovery of reaction -13 can resolve the huge discrepancy between the kinetic study of Elliot et al. and the steady-state radiolysis/product analysis study of Deeble et al., which reported only very slow reaction of H with I^-. In the reaction scheme assumed by Deeble et al., the H atoms may react irreversibly with either the halide ion or with 2-propanol-d_8 to give HD product. This competition should, in principle, reduce the amount of HD product. However, rate constants some two orders of magnitude smaller than those determined in our study were deduced for both ions. Clearly, if the HX^- product dissociates again on a short time scale, the liberated H atoms will all eventually react with 2-propanol-d_8, and the added halide ion will produce essentially no change in the HD product yield. The effective rate for k_{19} found in the competition experiment is naturally much smaller than the correct value.

In conclusion, our measurements have succeeded in establishing the H atom + halide reaction rates, and reconciling previous literature results in terms of the $H + X^- \rightleftharpoons HX^-$ equilibrium. The measured activation energies for the forward reaction are found to be far smaller than typically determined for reactions of small free radicals in aqueous solution, even though the rates are orders of magnitude smaller than the diffusion limit. It appears that the only reasonable explanation for this situation is in terms of a quantum-mechanical curve-crossing mechanism, involving orthogonal electronic states. (If the mixing of the states involved spin-orbit coupling, the heavier I^- atom would naturally react much faster than Br^-, as observed.) However, it is entirely unclear which electronic states might cross, given the gas-phase energetics and correlation diagrams of HX^- molecules. Apparently, the water solvent plays an intimate role in the process. This problem awaits further study.

3. Diffusion of H, D, and Muonium Atoms in Ice *D. M. Bartels, P. W. Percival*

In a previous year, we reported EPR spin-spin relaxation times, T_2, for H and D atoms generated in ice by electron pulse radiolysis over the temperature range 150-260 K. The dependence of this transverse spin relaxation on the ice H/D composition clearly demonstrated that the mechanism is purely electron-nuclear dipole relaxation, modulated by diffusion of the atoms through the lattice. An unfulfilled goal of the original study was the experimental measurement of longitudinal relaxation times, T_1, which would allow unequivocal determination of the motional correlation time, τ, from solution of the simultaneous equations:

$$\frac{1}{T_1} = \omega_L^2 \left(\frac{2\tau}{1+\omega_0^2\tau^2} \right) \tag{16}$$

$$\frac{1}{T_2} = \omega_L^2 \left(\tau + \frac{\tau}{1+\omega_0^2\tau^2} \right) \tag{17}$$

where ω_0 is the electron larmor frequency ($2\pi \times 9.27$ GHz in our experiment), and ω_L^2 is the second moment of the random magnetic field created by the lattice nuclei. The measurements of T_2 were already made difficult by the interference of Heisenberg spin exchange, a second-order spin relaxation mechanism resulting from diffusive encounters of the H and D atoms. Initial attempts to measure the much longer T_1 relaxation time proved futile because signal-to-noise was insufficient at the very low H-atom densities required to avoid the second-order spin relaxation process. Consequently, the T_2 data was modeled with ω_L^2 as an additional fitting parameter.

Analysis of the T_2 results suggested that it might be possible to measure the T_1 for H atoms under the most favorable circumstances, in H_2O ice near the melting point. We report here our measurement of both T_1 and T_2 at -6 °C, from which we deduce diffusional correlation times for H and D atoms in hexagonal ice.

H atoms were generated in a random polycrystalline ice sample in an EPR cavity by pulse radiolysis with 3 MeV electrons from a Van de Graaff accelerator. T_2 measurements were made by the two-pulse spin-echo method. T_1 measurements were made by a dynamic inversion recovery method. A 180° inversion pulse was applied at a time t_0 after the radiolysis pulse. The longitudinal magnetization was then measured at a later time t_0+t_{rec} by applying a 90° probe pulse, and integrating the first microsecond of the resulting FID.

In Figure 14, we illustrate the magnetization of H atoms in ice by plotting the initial FID amplitude as a function of time following pulse radiolysis at -6 °C. As can be seen, the H-atom EPR spectrum is immediately observed in a spin-polarized state, with low-field emission and high-field absorption (an E/A pattern) characteristic of CIDEP from random (F-pair) recombination reactions. The prompt appearance of this polarization implies significant cross recombination in radiolysis "spurs". Under the relatively low-dose conditions of this experiment, subsequent CIDEP generation from second-order recombination is slow, and the polarization decays slowly rather than growing quickly as demonstrated in our previous work. Unexpectedly, a small signal was still present immediately before each radiolysis pulse, left over from the pulse applied 2.8 ms previously.

Because the absolute signal amplitude persists much longer, inversion recovery and spin-echo experiments were performed on the high-field line. Inversion pulses were applied at t_0 = 50, 250, and 450 μs following radiolysis, and also at 200 μs before each radiolysis pulse to establish a baseline. In Fig. I-15, we show the (unexpected) small inverted (S_{rec}) and noninverted (S_{ref}) magnetization signals for the "baseline" scan at t_0 = -200 μs. Because the reference signal is very constant over this period, a recovery time T_r = 23.3 μs can be obtained from a simple exponential fit to the inversion recovery. The inversion pulse rotates the initial magnetization signal into its negative, so the true zero level can be deduced as halfway between the inverted and final signal levels, as shown. (This information was then used to establish the zero level in Figure 14, as well.) An identical experiment to the one illustrated in Figs. I-14 and I-15 was performed with the radiolysis dose (electron charge per pulse) cut by half. The recovery times averaged 23 μs. We appear to have successfully found a low-dose limiting dynamic inversion recovery time of 23 ± 3 μs. Strictly speaking, however, this should be regarded as a lower limit for T_r because we were not able to test the polarization recovery at even lower radiation dose.

In Figure 16 we plot a typical spin-echo envelope decay curve recorded at 50 μs after a slightly larger 12 ns, 2.8 nC radiolysis pulse, signal averaged at 180 ns Hz. The larger radiation dose could be used because T_2 is shorter than T_1, but signal/noise is comparable to the T_1 measurement because a shorter gate width (200 ns) is used to measure the peak amplitude of the spin echo. A weighted average of this and eight other measurements gives 6.9 ± 1.0 μs as the T_2 value for H atoms in ice at -6 °C.

By substituting the relaxation times determined at -6 °C, T_1 = 23 ± 3 μs and T_2 = 6.9 ± 1.0 μs into eqs. 16 and 17, it is possible to derive values for ω_L^2 and the correlation time at that temperature, namely

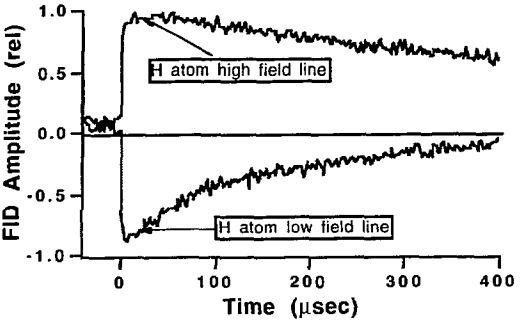

Figure 14. H-atom magnetization in ice at -6 °C, recorded as a function of time following pulse radiolysis (5 ns, ca. 400 rad pulses repeated at 360 Hz). The high-field (m_I = -1/2) line is polarized in absorption, and the low-field (m_I = +1/2) in emission (negative signal). The magnetization present immediately after the pulse is generated by CIDEP in cross-recombination reactions in radiolysis spurs. Just prior to each radiolysis pulse, a small signal remains from H atoms created in the previous pulse.

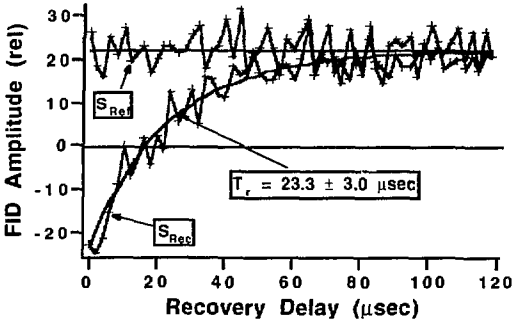

Figure 15. Dynamic inversion recovery of the H atom high-field line, in ice at -6 °C. On alternating radiolysis shots, a 70 ns microwave inversion pulse was applied to produce the "recovery" signal S_{rec}. This experiment is performed on the very small signal remaining some 2.8 ms after a 400 rad radiolysis pulse. The true "zero" level is inferred from half the initial difference in S_{ref}-S_{rec}.

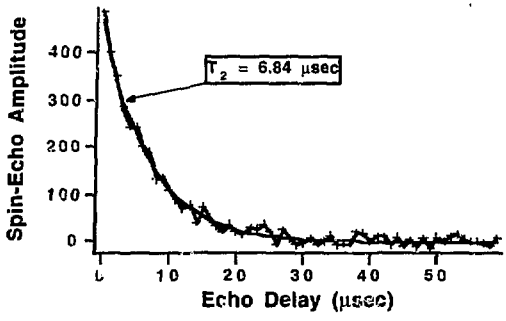

Figure 16. Spin-echo decay envelope of the H-atom high-field line in -6 °C ice at 50 μs following pulse radiolysis with ca. 700 rad radiation pulses. An average of nine similar curves at different time delays and on different days gave 6.9 ± 1.0 for our best estimate of T_2.

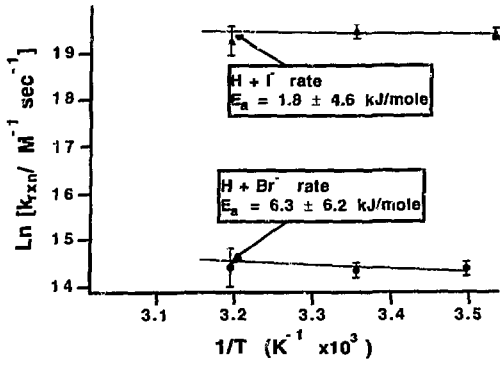

Figure 17. Diffusional correlation times for free H and D atoms in several isotopic mixtures of ice-Ih. The correlation times were calculated from transverse spin relaxation times on the basis of the calibration point at -6 °C, for which the spin-lattice relaxation time was also measured.

$\omega_L^2 = 3.3 \pm 0.7 \times 10^{15}\ s^{-2}$ and $\tau = 3.7 \pm 0.7 \times 10^{-11}$ s. This value of ω_L^2 was then used in eq. 17 to translate previous measurements of T_2 into motional correlation times of H over a range of temperatures. Furthermore, after correcting ω_L^2 for isotopic composition, the same procedure was used to deduce correlation times for H and D in other ices. The resulting values of τ are plotted in Figure 17.

The clearest difference is between H atoms and D atoms. Their behavior is best compared in the same lattice (90% D_2O), but even the other data sets reflect the higher activation energy and smaller τ_0 for H. Surprisingly, below ca. 200 K the D atom diffuses faster than the H atom. This unexpected inverse isotope effect was explained by using transition state theory. The adiabatic "bottleneck" at the transition state between minimum energy sites is more severe for H than D because of its higher zero-point vibrational energy. It is quite possible that the inverse isotope effect is a very general phenomenon in the diffusion of hydrogen in solids.

The high rate of H and D (and also Mu) diffusion in ice in the upper temperature range is a consequence of the open channel structure of the ice I_h lattice. Given the hopping rate at 273 K of $2.8 \times 10^{10}\ s^{-1}$ and the distance of 3.67 Å between minimum energy sites, one can calculate a one-dimensional c-axis diffusion coefficient of $1.9 \times 10^{-5}\ cm^2\ s^{-1}$. Remarkably, this diffusion coefficient is only about a factor of two smaller than that for liquid water close to the freezing point.

4. Solvent Relaxation Dynamics

Y. Lin, C. D. Jonah

The effects of solvation and solvent dynamics on chemical reactions and especially on charge-transfer processes have long been a subject of great importance in radiation chemistry. Much past work has involved comparing equilibrium solvation effects, probed by measuring the shift of optical absorption spectra, with chemical reactivity. However, chemical reactivity is a dynamic process, and solvation effects will vary as a function of time. The dynamics of the solvent can be observed by monitoring solvent response to the fast formation of different charge distributions (either a dipole or an ion) on a probe molecule. Solvation dynamics were first studied by observing the shift of the optical spectrum of the simplest ion, the electron. In the last decade, picosecond time-resolved absorption and emission spectroscopy have been used to measure the relaxation of the solvent around an excited state. Until our work, there had been little research on the solvation of charged species in room temperature fluids. This is a major deficiency because many chemical reactions in the condensed phase involve the creation or destruction of ions.

We have applied pulse radiolytic (PR) techniques to study the solvation of anions in polar media. In our approach, a high concentration of the probe molecule, benzophenone, which reacts very efficiently with the presolvated electron, is placed in the solution. Because the benzophenone reacts with the precursor of the solvated electron, the anion is formed very quickly. The advantage of the pulse radiolytic technique over the laser method is that it allows observations to be made on the ground state of the anion rather than on a short-lived excited state and, thus, one can measure long solvation times. Moreover, complications due to changing emission lifetimes as a function of wavelength, which can occur using laser techniques, are not encountered.

a. Pure Solvent Solvation Dynamics

The relaxation of the solvent polarization due to a sudden change in the charge distribution of a system has recently received much attention. Experimental and theoretical work have revealed the importance of the molecular structure of the solute and solvent in solvation dynamics.

We studied the dynamics of anion solvation in several dipolar, nonconducting solvents and, in what may be considered a major advance, measured the solvation time of anions in room temperature solvents. Previous work involved dipole solvation or electron solvation. Figure I-18 compares the solvation time of anions, electrons, and dipoles to the solvent longitudinal relaxation time τ_L. The solvation times obtained from electron solvation and anion solvation experiments are much faster than the solvation times of dipoles. These results clearly show the importance of measuring ion solvation rather than assuming that the solvation times will be similar to dipole solvation. The similarity of the solvation time of the anion and the electron (despite the quantum nature of the latter) shows up clearly, as do the differences between the solvation around an anion and a dipole (despite the similar molecular framework). The substantial difference shown in these measurements indicates that there are fundamental differences between the solvation of charged entities and dipoles.

We will expand this work to measure different probe molecules and different temperatures. We plan to study substituted benzophenone molecules that will change either the geometry around the anion or the interactions between the probe molecule and the solvent molecule. Variable-temperature experiments will be very useful for altering the solvation pathways. Because there are considerably different activation energies for different solvent molecule motions, measurements at different temperatures will make it possible to probe the different processes.

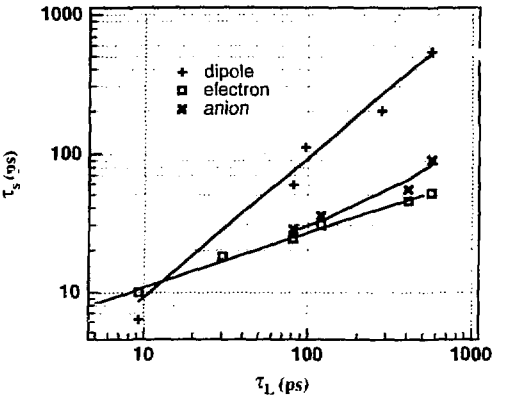

Figure 18. Solvation time of the benzophenone anion, the electron, and a dipole versus the longitudinal relaxation time of the solvent, τ_L.

b. Solvation Dynamics in Electrolyte Solutions

We have extended our work on the solvation dynamics of anions in dielectric fluids by studying solvation dynamics in electrolyte solutions. Although ionic effects are well known in chemistry, a quantitative theory does not exist for high ion concentrations. There will be an additional energetic relaxation process in ionic solutions. Adding to the stabilization by solvent molecular reorientation will be the energy lowering caused by the migration of electrolyte ions under the influence of the charge of the anion—an attraction for the electrolyte cations and a repulsion for the electrolyte anions. This will increase the field at the anion and be reflected in the absorption and emission spectra of the probe ion.

We have studied the dynamics of the benzophenone anion solvation from 100 ps to 50 ns in solutions of Li^+, Na^+, and Ba^{+2} in acetonitrile, propylene carbonate, and in methanol. The solvation of the anion is too fast to measure in methanol or acetonitrile. The absorption maximum of the species with equilibrium solvation is 720 nm in acetonitrile and 630 nm in methanol.

In the presence of an electrolyte in acetonitrile, the absorption maximum of the radical anion is significantly blue shifted and the dynamics are significantly slower. The transient absorption spectra of the benzophenone anion in 0.5 M $NaClO_4$ in acetonitrile are shown in Figure 19. The spectra were run at 2 ns, 5 ns, 10 ns, and 15 ns (from right to left), respectively. Data have also been taken using the stroboscopic pulse radiolysis system, and the spectral responses of the two systems have been corrected. The relaxation as a function of time for an anion in this salt-acetonitrile solution, as well as for several others, is displayed in Figs. I-20 and I-21. As is clear from these data, the relaxation time is considerably slower than in the pure acetonitrile. For example, the 0.5 M $NaClO_4$ solution has an exponential relaxation time of 2.4 ns, at least two orders of magnitude slower than the slowest time possible for the pure acetonitrile. As one can see from the figure, this behavior is typical for ionic solutions. These results show that the relaxation processes arising from the rotational motions of the solvent dipoles are much faster than the solvation from ion translation or migration, which occurs in the electrolyte solutions.

The two experimental observables that change in our experiments are the spectral shift (or the final spectral position) and the time for the spectral relaxation. These parameters depend both on the salt identity and the salt concentration, as can be seen in Figure 21. For example, for $NaClO_4$ the spectral shift increases and the solvation time decreases with an

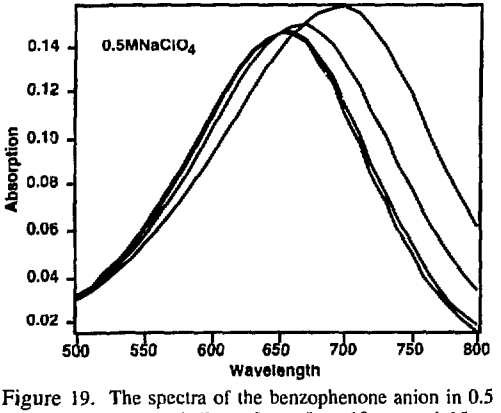

Figure 19. The spectra of the benzophenone anion in 0.5 M $NaClO_4$ in acetonitrile at 2 ns, 5 ns, 10 ns, and 15 ns after formation. The spectra show a blue shift as a function of time.

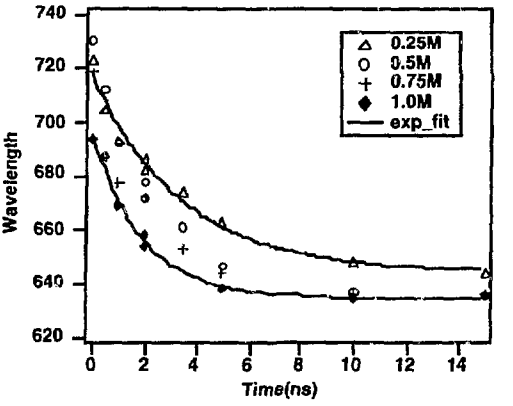

Figure 20. The peak of the absorption spectrum of the benzophenone anion vs. time for four different concentrations of $NaClO_4$ in acetonitrile.

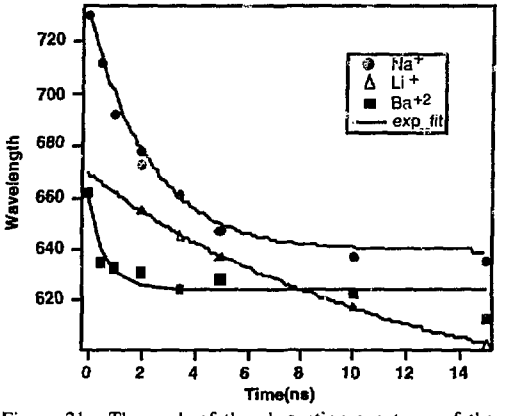

Figure 21. The peak of the absorption spectrum of the benzophenone anion vs. time for 0.5 M $NaClO_4$, $LiClO_4$, and $BaClO_4$ in acetonitrile.

increase in salt concentration. These results are summarized in Table 3.

In addition to the salt identity and concentration, a change in the solvent also changes the rate and amount of the spectral relaxation. These results are tabulated in Table 4 for $NaClO_4$ in a variety of solvents. There appears to be an inverse correlation between the amount of shift with the neat solvent and the additional shift with the added salt. For example, in methanol, where the spectral shift is large, the additional shift caused by the addition of the salt is small. In acetonitrile, where the pure solvent shift is small, the shift caused by the salt is large. These data

Table 3. Shift in the maximum of the spectrum, $\Delta\upsilon$, and solvation time, τ_S, of the benzophenone anion for different concentrations of $NaClO_4$ in acetonitrile.

concentration (M)	$\Delta n(cm^{-1})$	τ_S (ns)
0.25	1543	3.4
0.5	1809	2.4
0.75	1834	2.3
1.01	1859	1.9

Table 4. Solvation time and spectral shift for 0.25 M $NaClO_4$ in various solvents.

solvents	τ_S	$\Delta v(cm^{-1})$
methanol	<20 ps	~248
n-propanol	~70 ps	~248
acetonitrile	3.4 ns	1543
propylene carbonate	7.9 ns	919

may indicate that there is a limiting spectral shift, and, thus, additional solvating power may not shift the spectrum further. On the other hand, it may indicate that in a strongly solvating solvent (e.g., methanol) the electrolyte ion cannot replace a solvent molecule.

Two other groups have recently studied the influence of ions on the energetics and dynamics of dipole solvation by observing the time-dependent shift of the fluorescence spectrum. These experiments qualitatively agree with our observations in that the solvation in ionic solution is much slower than in the pure solvent, and that the relaxation dynamics depend not only on the solvent studied but also on the identity and concentration of the salt. The data have been interpreted using either a Debye-Falkenhagen ion-atmosphere approach (DF) or an ion-association (IA) model. The DF model is a continuum model whereas the IA model emphasizes specific interactions. We have analyzed our experimental measurements using these two different models, and, in agreement with previous workers, found that, at best, only qualitative agreement exists between theoretical predictions and the experimental data. The quantitative discrepancy of the existing models and experimental observations requires the development of more sophisticated molecular-level models that also can incorporate the continuum structure of the fluid.

c. Molecular Dynamics Simulations of Solvation in Pure Fluids

Theoretical studies were undertaken to model the results of experimental measurements of anion solvation times in alcohols. In alcohols, spectra of the equilibrium-solvated anion are virtually the same for n-butanol and n-decanol, and greatly different for n-butanol and 2-butanol. A continuum theory would have predicted the opposite—the spectra would be the same for the two butanols and greatly different for the n-butanol and n-decanol. We suggested that these results arise from the packing of the OH bonds around the anion and, using Monte Carlo techniques, showed that this explanation is reasonable.

Monte Carlo calculations do not probe the kinetics of solvation; instead, they only determine the equilibrium configurations. To calculate the solvation times, a molecular dynamics model was developed. Molecular dynamics simulations were performed for 216 solvent molecules and a single charged solute in the center of the simulation box. The dimension of the box is 23 nm. The simulation employed a cubic periodic boundary condition with the minimum-image convention. Initially, the solvent molecules were placed on a face-centered cubic lattice with lattice parameter 0.31 nm. The systems were studied in both a constant-energy and constant-temperature ensemble. The classical equations of motion were solved using a leapfrog scheme for linear rigid molecules. Time steps of 2 fs were used in the integration. All the simulations reported here were run at 300 K.

A linear rigid array of n atoms was used as a model of the solvent molecules. The dipole was modeled as partial charges, q+ and q-, on adjacent atoms with the positive charge always on the end of the molecule. The solvent molecules are electrically neutral. The short-range part of the intermolecular interaction was modeled by a Lennard-Jones potential between the atoms, and the long-range coulomb interactions between the charge groups of the solvent were calculated using a spherical approximation to the Ewald summation. The interaction parameters for both solvent and solutes are given in Table 5.

Both the orientation and the distance of the model solvent molecules from the central ion have been probed. We have carried out calculations for both a positive and a negative central ion. Figure I-22 shows the average orientation of the solvent molecules in

Table 5. Characteristics of the different solute and solvent properties simulated. For the solvent, σ(Å) will be the exclusion volume of the central ion in angstroms and q will be the charge in atomic units. For the solvent, σ(Å) is the diameter of each "atom" of the solvent, and E/k is the Lennard-Jones potential parameter for the "atom".

solute properties			solvent properties			
solute	σ(Å)	q(a.u.)	solvent	σ(Å)	E/k(K)	# of atoms
Q0	2.1	0	S2	3.5	190	2
Q1	2.1	1.0	S3	3.5	190	3
Q2	2.1	2.0	S4	3.4	190	4
Q3	2.1	-1				

the first solvation shell, $\langle\cos(\vec{\mu}\cdot\vec{r})\rangle$, where $\vec{\mu}$ is the direction of the dipole in the molecule, and $\vec{r}$ is the unit vector from the central ion to the center of the molecule. This average would be 1 if all the nearest molecules pointed directly toward the central ion, 0 if the molecule is perpendicular to the line from the central ion, and -1 if the positive end of the molecule points directly away from the central ion. For an anion, the molecules are directed towards the central ion, with stronger alignment for the longer molecules. The alignment around a cation is weaker and in the reverse direction. The results reflect the balance of energetic constraints: the advantage of close approach between the negative end of the solvent dipole and the central cation without colliding, and the repulsion between the cation and the positive end of the solvent dipole.

The distance distribution is given in Figure 23 for solvent molecules with lengths of two, three, and four molecular units. R is the distance from the central ion to the center of the dipole, and g(R) is the number of solvent dipoles in a unit volume at a distance R from the central molecule relative to the number that would be in the same volume if the solution were homogeneous (for a homogeneous solution g(R) would be 1). Note that all three model solvent molecules have their dipoles at the same distance from the central ion. This is consistent with the experimental data in that the shifts of the spectra are independent of the length of the molecules.

We calculated the potential at the solute molecule. These results are shown in Figure 24. For a negative central ion, the electric potential is virtually the same at the central ion, independent of the length of the solvent molecule. This agrees very well with the experimental results, which show that the spectrum of the equilibrium-solvated benzophenone anion is virtually identical for different primary alcohols. Thus, the results show that the local structure rather than the long-range structure is dominating the solvation energetics.

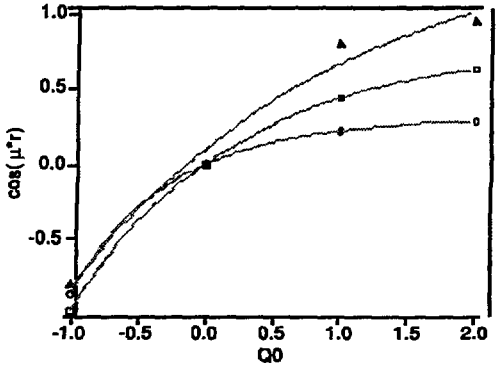

Figure 22. The average angle between the molecular dipole and the line between the center of the solvent molecule and the central charge. The lines are drawn only to guide the eye.

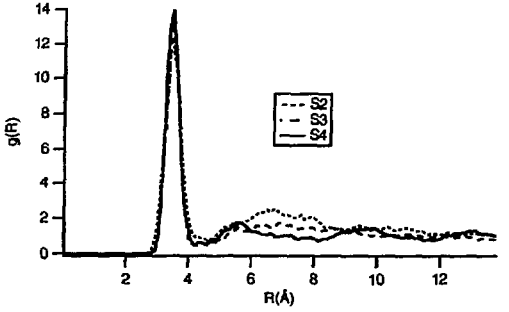

Figure 23. The radial distribution function g(R) as a function of distance R (in angstroms). R is measured from the central ion to the center of the dipole. S2, S3, and S4 are solvent molecules of length two, three, and four elements, respectively.

To study the solvation dynamics, the response of the solvent to an instantaneous change of the solute charge distribution is monitored. The solvent is equilibrated around a neutral solute molecule. The new

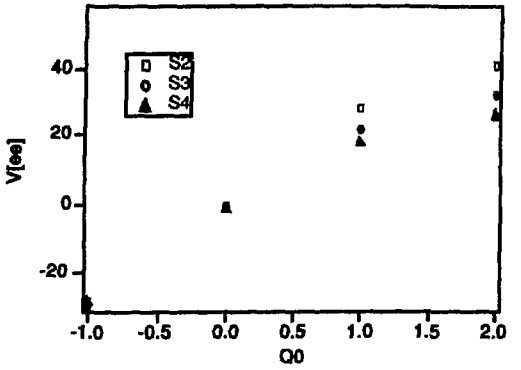

Figure 24. The potential at the central ion as a function of the central charge for solvent molecules of length two, three, and four elements.

charge distribution is imparted to the solute molecule, and the kinetic energy, rotational energy, and the potential at the solute molecule <V(t)> are observed for approximately 2 ps. To achieve reasonable statistics, this process is repeated about 500 times.

As can be seen in Figure 25, the solvation dynamics are slightly different for the relaxation around a cation and an anion. Common to all the systems studied, the dynamics show two components, a fast response of 0.1-0.2 ps and a slower relaxation of 1 ps or greater. The fraction of the fast relaxation is greater for the short molecules than for the longer molecules.

The short timescale can be thought to be due to inertial dynamics (mainly rotational) of the solvent

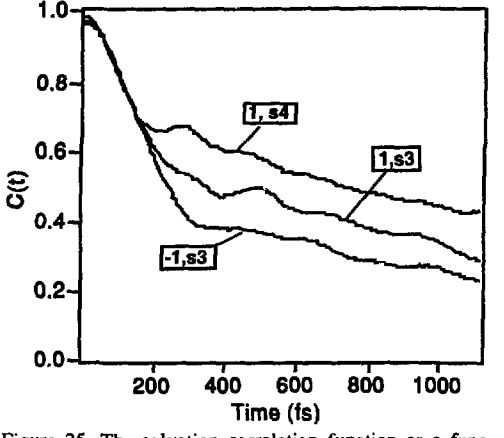

Figure 25. The solvation correlation function as a function of time for solvent molecules of three and four elements and as a function of the charge of the central ion.

molecule. That is, the solvent molecule is rotating and continues to rotate to reach the lowest potential. However, for longer molecules, the inertial rotation is small, because a molecule collides with other solvent molecules and the relaxation becomes diffusional.

These calculations are beginning to tell us about the origin of the observed dynamics and energetics. Future work will probe the specific interactions between the solvent molecules and the central probe molecule, which give rise to the spectral shift.

PUBLICATIONS

DIFFUSION OF ATOMIC HYDROGEN IN ICE-I_h
D. M. Bartels, P. Han, and P. W. Percival
Chem. Phys. Lett. 210, 129-134 (1993)

ELECTRON SPIN RESONANCE STUDY OF IRRADIATED POLYSTYRENE FIBERS
A. Pla-Dalmau, M. Barnabas, A. D. Bross, A. D. Trifunac
Polymer Preprints Am. Chem. Soc. 34, 343-344 (1993)

RADICAL CATIONS OF QUADRICYCLANE AND NORBORNADIENE IN POLAR ZSM-5 MATRICES: THERMAL RETRO DIELS-ALDER REACTION
M. V. Barnabas and A. D. Trifunac
J. Chem. Soc. Comm. 10, 813-814 (1993)

EARLY EVENTS IN RADIATION CHEMISTRY AND IN PHOTOIONIZATION
A. D. Trifunac, D. M. Loffredo, and A. D. Liu
J. Rad. Phys. Chem. 42, 967-972 (1993)

ELIMINATION AND ION-MOLECULE REACTIONS OF HEXAMETHYLETHANE AND TRIMETHYLBUTANE RADICAL CATIONS IN ZSM-5
M. V. Barnabas, D. W. Werst, and A. D. Trifunac
Chem. Phys. Lett. 204, 435-439 (1993)

QUADRICYCLANE AND NORBORNADIENE RADICAL CATIONS IN SILICALITE: COMPARISON WITH FREON MATRICES
M. V. Barnabas, D. W. Werst, and A. D. Trifunac
Chem. Phys. Lett. 206, 21-24 (1993)

PHOTOIONIZATION AND ENSUING ION-MOLECULE REACTIONS OF POLYCYCLIC AROMATIC HYDROCARBONS IN ALKANE AND ALCOHOL SOLUTIONS
A.-D. Liu, D. M. Loffredo, and A. D. Trifunac
J. Phys. Chem. 97, 3791-3799 (1993)

EPR MEASUREMENT OF THE REACTION OF ATOMIC HYDROGEN WITH Br^- AND I^- IN AQUEOUS SOLUTION
D. M. Bartels and S. P. Mezyk
J. Phys. Chem. 97, 4101-4105 (1993)

TRAPPED HOLES ON TiO_2 COLLOIDS STUDIED BY EPR
O. I. Micic, Y. Zhang, K. R. Cromack, A. D. Trifunac, and M. C. Thurnauer
J. Phys. Chem. 97, 7277-7283 (1993)

MULTI-PHOTON PROCESSES IN CYCLOHEXANE AND TRANS-DECALIN AND THE FORMATION OF HIGH MOBILITY CATIONS
A.-D. Liu, M. C. Sauer, Jr., and A. D. Trifunac
J. Phys. Chem. 97, 11265-11273 (1993)

ELECTRON CAPTURE RATE CONSTANTS FOR SOLUTES IN ALKANE LIQUIDS MEASURED BY TRANSIENT PHOTOCONDUCTIVITY
M. C. Sauer, Jr. and K. H. Schmidt
Rad. Phys. Chem., 43, 413 (1994)

SOLVENT EFFECTS IN NONPOLAR SOLVENTS: RADICAL ANION REACTIONS
D. W. Werst
Chem. Phys. Lett. 202, 101-107 (1993)

EARLY EVENTS FOLLOWING RADIOLYTIC AND PHOTOGENERATION OF RADICAL CATIONS IN HYDROCARBONS
D. W. Werst and A. D. Trifunac
Rad. Phys. Chem. 41, 127-133 (1993)

PICOSECOND DYNAMICS OF BENZOPHENONE ANION SOLVATION
Y. Lin and C. D. Jonah
J. Phys. Chem. 97, 295-302 (1993)

THE DEPENDENCE OF THE BENZOPHENONE-ANION SOLVATION ON SOLVENT STRUCTURE
Y. Lin and C. D. Jonah
J. Phys. Chem. 96, 10119-10124 (1992)

TRANSIENT ABSORPTION SPECTRA OF AROMATIC RADICAL CATIONS IN HYDROCARBON SOLUTIONS
A.-D. Liu, M. C. Sauer, Jr., D. M. Loffredo, and A. D. Trifunac
J. Photochem. Photobiol. A: Chem. 67, 197-208 (1992)

INVESTIGATION OF ELECTRON TRANSFER BETWEEN THE HEXAARYLBIIMIDAZOLE AND VISIBLE SENSITIZER
Y. Lin, A.-D. Liu, A. D. Trifunac, and V. V. Krongauz
Chem. Phys. Lett. 198, 200-206 (1992)

MECHANISM OF THE FORMATION OF TRANSIENT AROMATIC RADICAL CATIONS IN ALCOHOLS: LASER FLASH PHOTOLYSIS AND PULSE RADIOLYSIS STUDIES
A.-D. Liu, M. C. Sauer, Jr., C. D. Jonah, and A. D. Trifunac
J. Phys. Chem. 96, 9293-9298 (1992)

STUDIES OF ION SOLVATION USING PULSE RADIOLYSIS
C. D. Jonah and Y. Lin
Radiation Research: A Twentieth-Century Perspective, Vol. II: Congress Proceedings,
W. C. Dewey et al., Eds., Academic Press, Inc., 1992, pp. 63-68

EXPERIMENTAL INVESTIGATION OF THE DYNAMICS OF BENZOPHENONE ANION SOLVATION
C. D. Jonah and Y. Lin
Chem. Phys. Lett. 191, 357-361 (1992)

SUBMISSIONS

CHEMICAL CONSEQUENCES OF NON-HOMOGENEOUS ENERGY DEPOSITION BY IONIZING RADIATION
C. D. Jonah
Radiation Protection Dosimetry, in press

THE RATIO OF TRIPLET TO SINGLET EXCITED STATE FORMATION FROM ION RECOMBINATION IN THE RADIOLYSIS OF AROMATIC SOLUTES IN ALKANE LIQUIDS
M. C. Sauer, Jr. and C. D. Jonah
Rad. Phys. Chem., accepted, 1993

FDMR IN LOW-TEMPERATURE SOLIDS. PART I. THEORY
I. A. Shkrob and A. D. Trifunac
J. Phys. Chem. (1993)

FDMR IN LOW-TEMPERATURE SOLIDS. PART II. OBSERVATION OF WEAKLY-BOUND ELECTRONS
I. A. Shkrob, D. W. Werst and A. D. Trifunac
J. Phys. Chem. (1993)

VERY LOW TEMPERATURE STUDY OF RADICAL CATIONS OF QUADRICYCLANE AND NORBORNADIENE IN Na-ZSM-5 ZEOLITES
K. R. Cromack, D. W. Werst, M. V. Barnabas, A. D. Trifunac
Chem. Phys. Lett. (1993)

PHOTOINDUCED HOLE TRANSFER FROM TiO_2 TO METHANOL MOLECULES IN AQUEOUS SOLUTION BY ELECTRON PARAMAGNETIC RESONANCE
O. I. Micic, Y. Zhang, K. R. Cromack, A. D. Trifunac, and M. C. Thurnauer
J. Phys. Chem. (1993)

ENCOUNTERS OF H AND D ATOMS WITH O_2 IN WATER: RELATIVE DIFFUSION AND REACTION RATES
P. Han and D. M. Bartels
Proceedings, International Workshop on Ultrafast Reaction Dynamics and Solvent Effects,
P. Rossky and Y. Gauduel, Eds. (1993)

THE DYNAMICS OF ANION SOLVATION IN ALCOHOLS
Y. Lin and C. D. Jonah
Understanding Chemical Reactivity, J. Simon, Ed., Kluwer Publishing (1992)

SOLID-STATE FDMR FROM SUNDRY POLYOXYETHYLENE ALKYL PHENYL ETHERS: A VERIFICATION OF THE SINGLE-STEP ELECTRON TUNNELING AS A CAUSE OF THE CHARGE MOBILITY IN FROZEN RIGID SOLIDS AT 4-30 K
I. A. Shkrob and A. D. Trifunac
J. Phys. Chem. (1993)

OBSERVATION OF AN AROMATIC RADICAL ANION DIMER: $(C_{10}F_8)_2^{\bullet-}$
D. W. Werst
J. Am. Chem. Soc. (1992)

PRESENTATIONS

SPIN DYNAMICS, REACTION, AND DIFFUSION OF H AND D ATOMS IN WATER AND ICE
David M. Bartels
Argonne National Laboratory Chemistry Division Monday Morning Seminar Series
January 18, 1993

RADICAL IONS IN RADIATION AND PHOTOCHEMISTRY. MAGNETIC RESONANCE AND OTHER STUDIES
A. D. Trifunac
Plenary Lecture, The First Australian-Asian Conference on Radiation Science and Nucler Medicine
February 14-20, 1993

STRUCTURE AND DYNAMICS OF RADICAL CATIONS
A. D. Trifunac
Invited seminar, University of Sydney, Australia
February 15, 1993

RADICAL CATIONS IN PHOTOIONIZATION AND RADIOLYSIS
A. D. Trifunac
Invited seminar, University of Melbourne, Australia
February 25, 1993

HIGH ENERGY CHEMISTRY: PHOTOIONIZATION AND RADIOLYSIS
A. D. Trifunac
Invited seminar, Joint Physical/Theoretical and Organic Chemistry Series, Australian National University, Canberra, Australia
March 2, 1993

TRANSIENT SPECIES IN RADIATION AND PHOTOIONIZATION
A. D. Trifunac
Invited seminar, University of Brisbane, Brisbane, Australia
March 15, 1993

RADICAL IONS: INTERMEDIATES IN HIGH-ENERGY CHEMISTRY
D. W. Werst
Radiation Research Society - 41st Annual Meeting/North American Hyperthermia Society 12th Annual Meeting, Dallas, TX
March 20-25, 1993

ANION SOLVATION IN ALCOHOLS
C. D. Jonah and Y. Lin
Invited Speaker, Radiation Chemistry Laboratory, Japanese Atomic Energy Research Institute, Osaka, Japan,
March 29, 1993

ANION SOLVATION IN ALCOHOLS
C. D. Jonah and Y. Lin
Invited Speaker, Kyoto Institute ot Technology, Kyoto Japan
April 15, 1993

CLUSTER FORMATION IN THE IRRADIATION OF PALLADIUM AND PALLADIUM-SILVER SOLUTION
C. D. Jonah
Invited Seminar, Radiation Chemistry Laboratory, Japanese Atomic Energy Research Institute, Osaka, Japan,
April 19, 1993

CONSEQUENCES OF THE NON-HOMOGENEOUS DEPOSITION OF ENERGY IN RADIOLYSIS
C. D. Jonah
Invited Seminar, Radiation Chemistry Laboratory, Japanese Atomic Energy Research Institute, Osaka, Japan,
April 22, 1993

ANION SOLVATION IN ALCOHOLS
C. D. Jonah and Y. Lin
Invited Seminar, Hokkaido University, Sapporo, Japan
April 26, 1993

CONSEQUENCES OF THE NON-HOMOGENEOUS DEPOSITION OF ENERGY IN RADIOLYSIS
Invited Seminar, Tokyo University, Japan
April 30, 1993

CONSEQUENCES OF THE NON-HOMOGENEOUS DEPOSITION OF ENERGY IN RADIOLYSIS
Invited Seminar, Beijing Normal University, Beijing, China
May 3, 1993

ANION SOLVATION IN ALCOHOLS
Invited Seminar, Beijing University, Beijing, China
May 6, 1993

COMPARISON OF EARLY EVENTS IN RADIATION AND PHOTOCHEMISTRY
A. D. Trifunac
Invited talk, Miller Conference, Bowness-on-Windemere, UK
April 3-8, 1993

A LASER DRIVEN PICO (AND SUBPICO??) SECOND ELECTRON LINAC
A. D. Trifunac and C. D. Jonah
Invited talk, Miller Conference, Bowness-on-Windemere, UK
April 3-8, 1993

RADICAL CATIONS: KEY INTERMEDIATES IN HIGH ENERGY CHEMISTRY AND IN ZEOLITES
A. D. Trifunac
Chemistry Division Monday Morning Seminar Series, Argonne National Laboratory
April 26, 1993

THERMODYNAMICS AND TRANSPORT PROPERTIES OF THE HYDRATED ELECTRON
D. M. Bartels
IBM Research Facility, Zurich, Switzerland
May 5, 1993

EPR, SPIN DYNAMICS, AND DIFFUSION OF H AND D ATOMS IN WATER AND ICE
D. M. Bartels
Invited Speaker, Physical Chemistry Seminar, University of Zurich, Switzerland
May 6, 1993

EPR, SPIN DYNAMICS, AND DIFFUSION OF H AND D ATOMS IN WATER AND ICE
D. M. Bartels
Invited Speaker, Radiation Chemistry Seminar, Interuniversity Reactor Institute, Delft, The Netherlands
May 10, 1993

HYDROPHOBIC BARRIER IN THE REACTION OF H ATOMS WITH O_2 IN WATER
D. M. Bartels
Invited Speaker, International Research Workshop on Ultrafast Reaction Dynamics and Solvent Effects
Asnieres-sur-Oise, France
May 12, 1993

ELECTRON SPIN RESONANCE STUDY OF IRRADIATION POLYSTYRENE FIBERS
A. Pla-Dalmau, M. Barnabas, A. D. Bross and A. D. Trifunac
ACS National Meeting, Chicago, IL
August 22-27, 1993

EPR MEASUREMENT OF THE DIFFUSION OF H AND D ATOMS IN ICE
D. M. Bartels
ACS National Meeting, Chicago, IL
August 22-27, 1993

THERMODYNAMICS AND TRANSPORT PROPERTIES OF THE HYDRATED ELECTRON
David M. Bartels
Invited Seminar, Department of Chemistry, Johns Hopkins University, Baltimore, MD
October 4, 1993

DYNAMICS OF ION SOLVATION
Y. Lin
Chemistry Division Monday Morning Seminar Series, Argonne National Laboratory
November 1, 1993

THERMODYNAMIC, TRANSPORT AND REACTIVITY PROPERTIES OF THE HYDRATED ELECTRON
David M. Bartels
University of Notre Dame, Notre Dame, IN
November 18, 1993

RADICAL ION REACTIONS STUDIED BY MATRIX-ISOLATION AND TRANSIENT METHODS
David Werst
Chemistry Division Monday Morning Seminar Series, Argonne National Laboratory
November 29, 1993

COLLABORATIONS

R. Cooper, University of Melbourne, Australia
Studies of transient species created in gases, liquids, and solids are being carried out. Recent efforts have concentrated on the spectra and dynamics of excited species created in solids, such as sapphire, which are investigated via time-resolved measurements of emitted light using the techniques of pulse radiolysis and laser flash photolysis. Sapphire is a prime contender for a lining material of the containment vessel in fusion reactions, and these studies are useful in understanding radiation effects.

B. Garrett, Battelle Pacific Northwest Laboratory, Richland, WA
Theoretical modeling of H-atom reactions in gas phase and water is being pursued.

S. Mezyk, Atomic Energy of Canada, Ltd., Pinawa, Canada
Reaction rates of H atoms with I^- and other iodine-containing solutes are being measured for the purpose of predicting the spread of radioactive iodine in potential nuclear accidents.

P. W. Percival, Simon Fraser University and TRIUMF, Burnaby, British Columbia, Canada
Investigation of H and D atoms in ice by time-resolved EPR has allowed determination of diffusion rates, and the development of a model H atom-H_2O interaction potential. The aim of the collaboration is improved understanding of H-atom transport and reactivity in solid lattices.

E. Roduner, Physical Chemistry Institute, Zurich University, Switzerland
Reaction of H atoms with benzene in water has been investigated in a test of the validity of transition state theory for reactions in aqueous solution. Precision measurements of the hyperfine coupling of H and D atoms in water have been made to elucidate the nature of hydrophobic hydration and effects of water "structure" on reaction rates.

C. Romero, University of Santiago, Chile
The properties of the hydrated electron are being studied via molecular dynamics simulations. A computational program has been developed to simulate aqueous LiCl solutions, and the results are compared to the experimental optical absorption spectrum. Water molecules are treated classically, and the electron is given a full quantum treatment. This is an important step towards simulating chemical reactions in ionic solutions.